Check for updates

AGU100 ADVANCING EARTH AND SPACE SCIENCE

JGR Oceans

RESEARCH ARTICLE
10.1029/2018JC014459

**Key Points:**
- Simulated convection events in years 2008, 2012, and 2014–2016 resulted in LSW formation rates of 3.5, 5.1, 1.25, 2, and 7 Sv, respectively
- Increased Greenland melt and precipitation impact denser LSW replenishment; the overall LSW formation rate and maximum MLD did not decrease
- Potential decreases in Labrador Sea winter heat loss due to global warming may be a bigger threat to LSW formation than freshwater increase

**Correspondence to:**
Y. Garcia-Quintana,
yarisbel@ualberta.ca

**Citation:**
Garcia-Quintana, Y., Courtois, P., Hu, X., Pennelly, C., Kieke, D., & Myers, P. G. (2019). Sensitivity of Labrador Sea Water formation to changes in model resolution, atmospheric forcing, and freshwater input. *Journal of Geophysical Research: Oceans*, *124*, 2126–2152. https://doi.org/10.1029/2018JC014459

Received 12 AUG 2018
Accepted 22 FEB 2019
Accepted article online 28 FEB 2019
Published online 28 MAR 2019

©2019. American Geophysical Union. All Rights Reserved.

# Sensitivity of Labrador Sea Water Formation to Changes in Model Resolution, Atmospheric Forcing, and Freshwater Input

**Yarisbel Garcia-Quintana[1], Peggy Courtois[1], Xianmin Hu[1,2], Clark Pennelly[1], Dagmar Kieke[3,4], and Paul G. Myers[1]**

[1]Department of Earth and Atmospheric Sciences, University of Alberta, Edmonton, Alberta, Canada, [2]Ocean Sciences Division, Department of Fisheries and Oceans, Bedford Institute of Oceanography, Dartmouth, Nova Scotia, Canada, [3]Institute of Environmental Physics, University of Bremen, Bremen, Germany, [4]MARUM-Center of Marine Environmental Sciences, University of Bremen, Bremen, Germany

**Abstract** Labrador Sea Water (LSW) is one of the main contributors to the lower limb of the Atlantic Meridional Overturning Circulation. In this study, we explore the sensitivity of LSW formation to model resolution, Greenland melt, absence of high-frequency atmospheric phenomena, and changes in precipitation. We use five numerical model simulations at both (1/4)° and (1/12)° resolutions. A kinematic subduction approach is used to obtain the LSW formation rate over the period 2004 to 2016. The control simulation, with (1/4)° resolution, showed a mean annual production rate of 1.9 Sv (1 Sv = $10^6$ $m^3/s$) in the density range of 27.68–27.80 $kg/m^3$ for the period 2004–2016. Deep convection events that occurred during 2008, 2012, and 2014–2016 were captured. We found that with (1/4)° resolution the LSW formation rate is 19% larger compared with its counterpart at (1/12)° resolution. The presence of Greenland melt and an increase in the precipitation impact the denser LSW layer replenishment but do not decrease the overall LSW formation rate nor the maximum convection depth. A dramatic response was found when filtering the atmospheric forcing, which induced a decrease of 44% in heat loss over the Labrador Sea, strong enough to halt the deep convection and decrease the LSW formation rate by 89%. Even if our experiment was extreme, a decrease in the storms crossing the Labrador Sea with a consequent reduction in the winter heat loss might be a bigger threat to deep convection and LSW formation in the future than the expected increases in the freshwater input.

**Plain Language Summary** The Labrador Sea, located between Greenland and Canada, is where strong winter cooling makes the surface waters lose heat to the atmosphere, get denser, and sink to depths between 500 and 2,500 m. This sinking brings heat and dissolved gases like oxygen and carbon dioxide into the deep ocean. The resulting water mass is known as Labrador Sea Water (LSW). The process through which LSW is formed is sensitive to freshwater inflow into the formation region and storms passing over the Labrador Sea. While an increase in freshwater would inhibit the densification and sinking of surface water, fewer storms would reduce heat loss also reducing the ability of the surface waters to gain in density and sink to greater depths. These are all changes projected to occur due to the ongoing anthropogenic climate change. By using a numerical model, we explore how the increase in freshwater from Greenland melt and precipitation, and the absence of storms could impact LSW formation. We found that by having more freshwater going into the formation region the overall LSW formation rate does not decrease, however, the water mass becomes lighter. In the absence of the storms, the formation rate drastically decreased.

## 1. Introduction

The subpolar North Atlantic is a vital area for heat and freshwater exchange between the low and high latitudes. Within the subpolar North Atlantic, the Labrador Sea, located between the Labrador coast of Canada and Greenland, exerts a significant influence on the climate system. In the basin strong oceanic heat loss during winter (Holdsworth & Myers, 2015; Jung et al., 2014; Schulze et al., 2016) together with a strong cyclonic circulation (e.g., The Lab Sea Group, 1998), induces deep convection, which during severe winters can reach water depths of 2 km (e.g., Yashayaev et al., 2008; Yashayaev & Loder, 2009, 2017). The resulting

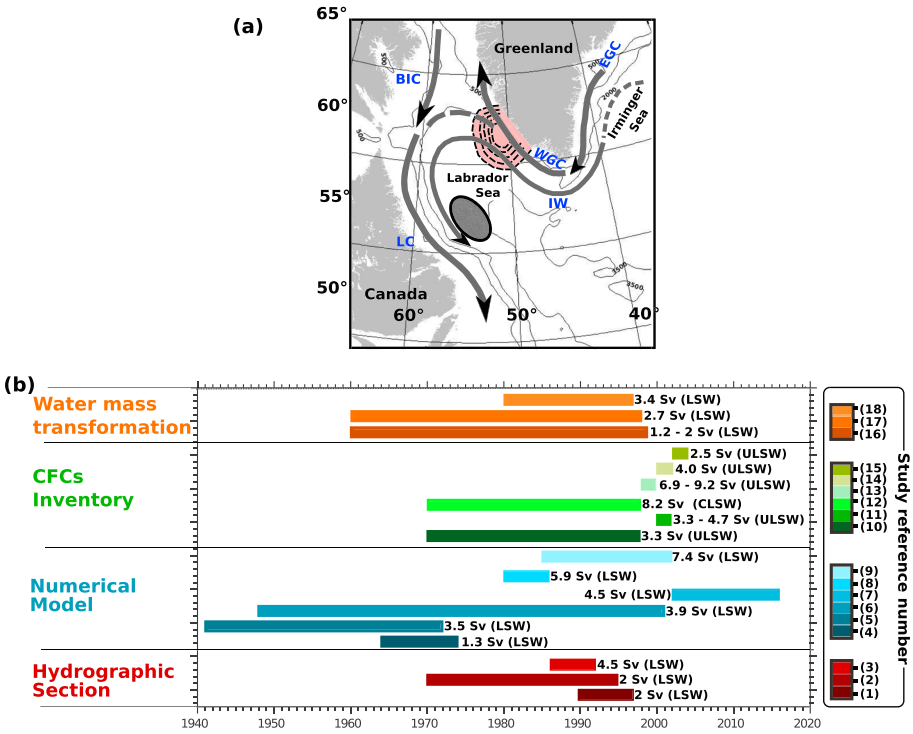


**Figure 1.** (a) Schematic showing the boundary current system around the Labrador Sea: East Greenland Current (EGC), West Greenland Current (WGC), Irminger Water (IW), Baffin Island Current (BIC), and Labrador Current (LC). Also displayed in this sketch is the deep convection region (shaded ellipse) after The Lab Sea Group (1998), the region with the higher incidence of eddies shed out of the WGC (pink region contoured by black dashed lines) after Chanut et al. (2008), and the isobaths 500, 2,000, and 3,500 m. Panel (b) summarizes the results from different studies investigating Labrador Sea Water (LSW) formation rates using four methods: Hydrographic observations, numerical model output, chlorofluorocarbons (CFCs) inventories, and water mass transformation approach. Each horizontal bar indicates the study period of the responding study (labeled with color). The resultant rate is notated adjacent to the bar. The color scales on the right refer to the studies listed as follows: (1) Pickart and Spall (2007), (2) Yashayaev et al. (2004), (3) Yashayaev and Clarke (2006), (4) Khatiwala and Visbeck (2000), (5) Böning et al. (1996), (6) Gerdes et al. (2005), (7) Courtois et al. (personal communication, 2018), (8) Mauritzen and Häkkinen (1999), (9) Marsh et al. (2005), (10), (11) and (13) Kieke et al. (2006), (12) LeBel et al. (2008), (14) and (15) Kieke et al. (2006), (16) Myers and Donnelly (2008), (17) Khatiwala et al. (2002), and (18) Marsh (2000). ULSW = Upper Labrador Sea Water.

product of the deep convection is Labrador Sea Water (LSW). LSW is the lightest component of the North Atlantic Deep Water, which feeds the deep and abyssal limb of the Atlantic Meridional Overturning Circulation (AMOC; e.g., Haine et al., 2008; Rhein et al., 2015). Once formed, LSW spreads out from its formation region loaded with high concentrations of dissolved oxygen and anthropogenic tracers like chlorofluorocarbons and can be tracked throughout the entire North Atlantic and beyond (e.g., Dickson et al., 2007; Kieke & Yashayaev, 2015; Rhein et al., 2002, 2015).

In the upper layer of the Labrador Sea, the Labrador Current and West Greenland Current (LC and WGC, respectively) pass around the Labrador Sea margins (Figure 1a). These two currents form a counterclockwise boundary current, carrying sea ice, icebergs, and low-salinity water from the Arctic as well as runoff from North America and the Greenland ice cap (e.g., Dickson et al., 2007; Yang et al., 2016; Yashayaev et al., 2008; Yashayaev & Dickson, 2008). Warm and salty waters from the Irminger Current are also advected into the Labrador Sea (McCartney & Talley, 1982). The Irminger Water (IW) is a component of the boundary current system found in the Labrador Sea. It can be identified around the rim of the basin (Figure 1a), and its core can be found at a depth range of 200 to 1,000 m over the slope (Myers et al., 2007).

Along the Greenland side, boundary current instabilities result in the formation of Irminger Rings (IR) (see, e.g., de Jong et al., 2014; Lilly et al., 2003; Figure 1a). These warm-core eddies have a diameter of 30–60 km and are known to contribute to the overall heat and salt budget of the basin (Lilly et al., 2003; Yashayaev,

2007), playing an important role during the restratification phase after the winter convection in the Labrador Sea (de Jong et al., 2014; Hátún et al., 2007; Gelderloos et al., 2011).

Convective eddies (CE) are also known to play an important role during the restratification phase (Marshall & Schott, 1999). After convection, baroclinic instability generated by the strong density differences between the mixed patch and the ambient fluid breaks up into cold CE with a diameter between 10 and 36 km (Lilly et al., 2003). The CE mix the upper water column, while the denser and mixed water core spreads along isopycnals at depth (Gelderloos et al., 2011; Marshall & Schott, 1999).

The boundary current system encircling the Labrador Sea is also associated with the doming of the isopycnals toward the center of the basin. This brings water weakly stratified from the interior of the basin closer to the surface, reducing the stratification and setting favorable conditions for deep convection to occur (The Lab Sea Group, 1998).

The critical role played by the boundary currents and the eddies, which result from them makes model resolution an important feature to investigate the LSW formation. Chanut et al. (2008) compared different model experiments with a horizontal resolution of (1/3)° and (1/15)° to investigate the role of mesoscale eddies in the variability of deep convection in the Labrador Sea. By using the (1/15)° horizontal resolution experiment, they were able to have a better representation of IR, CE and boundary current eddies (BCE), the interior heat budget of the Labrador Sea, and therefore the variability of deep convection. Also, Marzocchi et al. (2015) found that when the resolution of the model is increased the boundary currents are better represented, and thus the advection processes within.

The variability of LSW formation has been widely analyzed (see, e.g., Azetsu-Scott et al., 2003; Houssais & Herbaut, 2011; García-Ibáñez et al., 2015; Kieke & Yashayaev, 2015; Rhein et al., 2011; Yashayaev et al., 2007). Such variability is known to be closely linked to changes in the atmospheric forcing (see, e.g., Holdsworth & Myers, 2015; Schulze et al., 2016) particularly to the phases and persistence of the North Atlantic Oscillation (NAO; e.g., Dickson et al., 1996; Kieke & Yashayaev, 2015; Yashayaev et al., 2008). During the positive phase of the NAO there is a stronger mean cyclonic flow over the North Atlantic Ocean and an increased circulation of cold air out of the Canadian Arctic. This generally leads to stronger heat loss over the Labrador Sea and hence deep convection (Hurrell & van Loon, 1997). During the negative phase of the NAO the situation reverses, resulting in mild winters that leads to a decrease in the heat loss over the Labrador Sea and reduced convective renewal of LSW (Hurrell & van Loon, 1997). However, this is not a one-to-one relation as even during negative NAO years deep convection can occur due to the "memory" of the previous winter preconditioning of the water column (Lazier et al., 2002). The years with negative NAO are also linked to the advection of freshwater into the Labrador Sea exported from the Arctic Ocean through Fram Strait, events that are known to have a negative impact on the winter deep convection (e.g., Dickson et al., 1988; Gelderloos et al., 2012; McCartney & Talley, 1982).

Besides the freshwater exported from the Arctic Ocean, there are local sources known to have an influence on the freshening of the basin: an increase in the melting of Greenland Ice Sheet (GrIS; e.g., Bamber et al., 2012; Brunnabend et al., 2015) and in precipitation (e.g., Myers, 2005). In fact, a likely consequence of global warming is the increment of freshwater discharge due to ice melting or precipitation increase, adding freshwater into the ocean with the subsequent risk of substantial changes in ocean circulation. If transported into the interior of the Labrador Sea, such freshwater discharges would reduce the surface salinity (Josey & Marsh, 2005), contributing to the stability of the water column and potentially reducing deep water formation.

High-frequency atmospheric phenomena such as cold-air outbreaks, polar lows, mesoscale cyclones, fronts, topographic jets,and extreme winter events in general, known to impact the convection depth (Holdsworth & Myers, 2015), are also expected to change with future climate warming (e.g., see details in Kolstad & Bracegirdle, 2008; Zahn & von Storch, 2010) and questions about how the ocean will respond to those changes are arising (Holdsworth & Myers, 2015).

The formation and downstream spreading of LSW and its contribution to the North Atlantic Deep Water make the North Atlantic Ocean the only basin among the world's ocean where large concentrations of anthropogenic $CO_2$ penetrate mid and abyssal depths (Sabine et al., 2004). At the same time strong oxygen intake occurs during deep convection events. As the mixed layer (ML) deepens it progressively exposes large volumes of undersaturated water to the atmosphere allowing the ventilation of the deep ocean (e.g.,

Kieke & Yashayaev, 2015; Stendardo & Gruber, 2012). So changes in LSW production, its properties, and thickness would have a direct impact on the potential of the ocean to store anthropogenic carbon (see, e.g., Steinfeldt et al., 2009) and on the ventilation of the deep ocean. Given its relevance various efforts have been made to investigate the LSW formation rate using numerous methods (chlorofluorocarbons inventories, numerical models, hydrographic changes, mass budget, heat budget, etc.). Haine et al. (2008) summarized various methods to infer the LSW formation rate and its variability, based on studies published between 1990 and 2008. The formation rates from some of those studies (in Haine et al., 2008), among others, are illustrated in Figure 1b. Therein, our main goal is to illustrate some of the different methods used to study the formation of LSW together with the associated rates and to use them to place our subduction estimates in context. For more details on the specifics of the methods and LSW definition used in the different studies, please refer to the manuscripts cited in Figure 1b.

The kinematic subduction approach has been used as a tool to investigate the ventilation of the ocean as well as water mass formation (e.g., Courtois et al., personal communication, 2018; Da Costa et al., 2005; Liu & Wang, 2014; Trossman et al., 2009). The approach integrates the local subduction rate over outcrop areas and over density classes. In principle, it is similar to the transformation approach (Marsh, 2000) but with consideration of advection. It quantifies the transfer of water below the ML into the deeper layers, effectively connecting the atmosphere to the ocean interior. One of the main advantages of the method is that it considers transfer into the ocean interior over a specific density range (Da Costa et al., 2005).

In this study we explore the impact of enhanced freshwater discharge (either by glacial melting or precipitation increase), high-frequency atmospheric forcing and model resolution on LSW formation by using numerical model output. We use the kinematic subduction approach to quantify the LSW formation rate in the period 2004 to 2016. To our knowledge this study is the first to use this method to investigate the variability of the LSW formation rate under different sensitivity experiments while using hourly atmospheric forcing data that allows the representation of a wide range of atmospheric phenomena. The study is preceded by Courtois et al. (personal communication, 2018) who, by using a high-resolution numerical simulation, investigated the subduction rate in the Labrador Sea from 2002 to 2014.

These different scenarios covered in the present manuscript were selected to investigate how the LSW formation might respond under changes predicted to occur due to the ongoing global warming (except in the case of model resolution): increase in GrIS melt, decrease of precipitation over the midlatitudes, and the decrease of high-frequency atmospheric phenomena over the Labrador Sea together with a poleward shift of the extratropical storm track. In the case of *SPG12* we were looking to tackle how the model resolution might impact the results. Numerical ocean models play an important role in increasing our ability to comprehend oceanic processes, monitor the current state of the oceans, and, to a limited extent (for now), even predict their future state.

Holdsworth and Myers (2015) also investigated the influence of high-frequency atmospheric forcing on the deep convection of the Labrador Sea using model output from 2002 to 2010 (for details see Holdsworth & Myers, 2015). One of the main differences between their and the present study is that they explored the impact on the convective energy in the Labrador Sea, while we investigate the influence on the LSW formation rate.

In order to explore the sensitivity of the LSW formation rate on changing conditions, a control simulation and four perturbation experiments were carried out using a state-of-the-art coupled ocean-sea ice model, run from 2002 to 2016. Each of the perturbation experiments has a specific alteration compared to the *Control* simulation. The model and a description of the experiment setup are introduced in section 2. Section 3 gives a detailed description of the kinematic subduction approach used to estimate the LSW formation rates. Section 4 describes the results obtained with the different experiments. Section 5 covers the discussion and conclusions.

## 2. Model Description and Experiments Setup

This section describes the details of the model and the configuration used. The different simulations used within each of the sensitivity experiments are also introduced.

### 2.1. Ocean-Sea Ice Model

The model used is the Nucleus for European Modelling of the Ocean (NEMO) numerical framework version 3.4 (Madec, 2008). The sea ice module is the Louvain-la-Neuve LIM2 (Fichefet & Maqueda, 1997). The

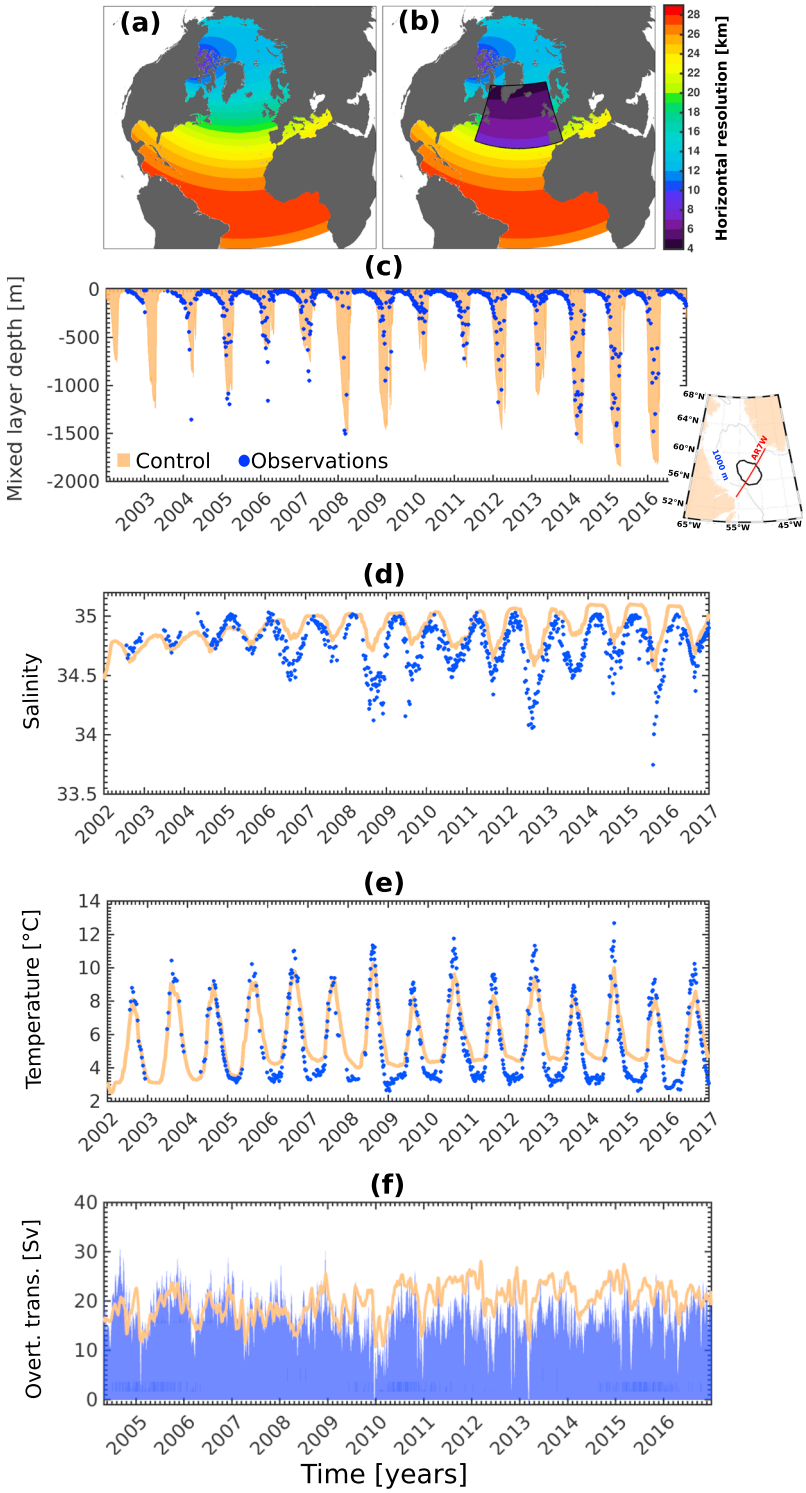


**Figure 2.** Horizontal resolution for (a) the ANHA4 domain and for (b) *SPG12*. The next panels show a comparison of the Control simulation and observations regarding (c) mixed layer depth and over the mixed layer depth averaged (d) salinity and (e) temperature, all over the black-contoured region in the map inset in (c) (Control vs. Argo floats), and (f) overturning transport (Overt. trans.) at 26.5°N (Control vs. RAPID array).

configuration used to run all the simulations in this paper is called *Arctic and Northern Hemisphere Atlantic* (ANHA) with a (1/4)° resolution (ANHA4; Figure 2a). The configuration covers the whole Arctic Ocean, North Atlantic, and a part of the South Atlantic with two open boundaries, one close to Bering Strait and the other one at 20°S. Its mesh grid is extracted from the (1/4)° global tripolar grid, ORCA025 (Barnier et al., 2007). The highest horizontal resolution (~6 km) is in Dease Strait, an east-west waterway between the mainland of Kent Peninsula and Victoria Island in Nunavut, Canada. The lowest resolution (~28 km) is at the equator. Over the Labrador Sea the horizontal resolution is around 16 km. The configuration has 50 vertical levels, with the layer thickness smoothly increasing from 1.05 m at the surface, to 453.13 m in the last level. No temperature or salinity restoring is applied, leaving the model to evolve freely without constraining the drift.

ANHA4 initial temperature, salinity, horizontal velocities (zonal and meridional), and sea surface height fields are obtained from *Global Ocean Reanalysis and Simulations* (GLORYS2v3) from MERCATOR (Masina et al., 2017). The initial ice field is a combination of GLORYS2v3 simulation and satellite observations. Lateral open boundary conditions (salinity, temperature, and horizontal velocities) are also from GLORYS2v3. This approach helps to reduce the model spin-up time by starting from a spun-up realistic state. GLORYS2v3 is a global ocean reanalysis produced by the MyOcean Global Monitoring and Forecasting Centre. The reanalysis is built to be as close as possible to the observations (i.e., realistic) and in agreement with the model physics. Using NEMO 3.1 and LIM2 EVP (elastic–viscous–plastic) sea ice model, GLORYS2v3 runs from January 1993 to December 2013. The mesh grid is extracted from ORCA025. It has 75 vertical levels and an eddy-permitting horizontal resolution of (1/4)°. It uses 3-hourly ERA-Interim as atmospheric forcing as well as bulk Coordinated Ocean-ice Reference Experiments formulation with radiative flux correction and diurnal cycle. The data assimilated in GLORYS2v3 includes the following: sea surface temperature (Reynolds AVHRR-AMSR (Advanced Very High Resolution Radiometer and Advanced Microwave Scanning Radiometer) (1/4)°), reprocessed sea surface height (Jason1, Jason2, Envisat, T/P, GFO, and ERS1-2), reprocessed in situ temperature and salinity vertical profiles from the Coriolis Data Center, CNES-CLS MSSH (Rio 2009), and sea ice concentration (Cersat). For more details on GLORYS2v3 please refer to the website (https://www.mercator-ocean.fr/wp-content/uploads/2015/08/FS-GLORYS2V3_EN.pdf).

The atmospheric forcing data used in ANHA4 come from the *Canadian Meteorological Centre's Global Deterministic Prediction System* (CGRF; Smith et al., 2014). CGRF provides 10-m surface wind, 2-m air temperature and specific humidity, downward longwave and shortwave radiation fluxes, and total precipitation. This data set has a temporal resolution of one hour and a spatial resolution of 0.45° in longitude and 0.3° in latitude (which is still relatively coarse compared to the ANHA4 spatial resolution). The Coordinated Ocean-ice Reference Experiments bulk formulae were applied to compute fluxes of heat, water, and momentum (Large & Yeager, 2009).

Monthly interannual river discharge from the 1° by 1° Global River Flow and Continental Discharge Dataset (Dai & Trenberth, 2002; Dai et al., 2009) is volume-conserved remapped onto the model grid. The original data set goes up to 2007, after that the runoff from 2007 is repeated. The river discharge from the adjacent areas of the Labrador Sea was found to be 117.9 $km^3$/year in this data set. Freshwater fluxes from Greenland (liquid component only) are based on Bamber et al. (2012). The liquid freshwater fluxes from Greenland goes up to 2010, and afterward the runoff from 2010 is repeated.

The regional configuration ANHA4 has been used in the past by Holdsworth and Myers (2015) to explore the influence of high-frequency atmospheric forcing on the circulation and deep convection in the Labrador Sea. Dukhovskoy et al. (2016) used the same configuration to look at the spreading of Greenland freshwater in the sub-Arctic Seas, while Gillard et al. (2016) explored the pathways of the melt-water from marine terminating glaciers of the GrIS. Müller et al. (2017) used the ANHA4 configuration to explore the temperature flux carried by individual eddies across 47°N in the Atlantic Ocean. They ran two different simulations using the ANHA4 configuration: one simulation with a horizontal resolution of (1/4)° over the entire domain and a second simulation with a two-way nest over the subpolar gyre to increase the horizontal resolution to (1/12)°. Both simulations, called ANHA4 and ANHA4-SPG12 (in Müller et al., 2017), are used in the present study. Here nevertheless they will be found under the names Control and SPG12, respectively.

### 2.2. Sensitivity Experiments Setup

Four perturbation experiments from a Control simulation were carried out using ANHA4 (Table 1): *Subpolar Gyre (1/12)° (SPG12)*, *Greenland Melt Removed*, *Filtered*, and *Precipitation Decreased (PD)*. All the

**Table 1**
*Set of Simulations Used in the Present Study*

| Simulation name | Horizontal resolution | Atmospheric forcing | Greenland and river runoff |
|---|---|---|---|
| Control | (1/4)° | CGRF | Interannual-Monthly with Greenland melt |
| SPG12 | **(1/12)°** | CGRF | Interannual-Monthly with Greenland melt |
| GMR | (1/4)° | CGRF | **Interannual-Monthly with Greenland melt removed** |
| Filtered | (1/4)° | **CGRF (••)** | Interannual-Monthly with Greenland melt |
| PD | (1/4)° | **CGRF (•)** | Interannual-Monthly with Greenland melt |

*Note. Control* (reference simulation), *SPG12* (horizontal resolution increased to (1/12)°), *Greenland Melt Removed* (GMR), *Filtered* (filtered winds and temperature fields), and *Precipitation Decreased* (PD). Bold emphasis is used to show what is different between the simulations of an experiment. CGRF (•) refers to a version of the atmospheric forcing containing a decrease in precipitation. CGRF (••) refers to the filtered (temperature and wind fields) version of the atmospheric forcing. The period considered for all the experiment was 2004 to 2016.

simulations, including the control run, were run from 1 January 2002 to 31 December 2016, with a temporal output resolution of 5 days. No leap years were considered as it is traditionally done for ocean models.

The perturbation experiment SPG12 was designed to evaluate the impact of the spatial resolution when calculating the LSW formation rate. To increase the resolution from (1/4)° to (1/12)°, two-way nesting was implemented using the *adaptive grid refinement in Fortran90* (Blayo & Debreu, 1999; Debreu et al., 2008; Laurent et al., 2005). The nest was centered over the region of the subpolar gyre, approximately between 36° to 68°N and 60°W and 10°E, with the ANHA4 configuration as the parent domain (Figure 2b). SPG12 was forced using the same collection of data sets used to force Control. The river runoff data set was interpolated to (1/12)°, though additional care was taken to ensure that all river runoff enters ocean grid cells. While the resulting spatial area where runoff is applied to the ocean may differ slightly between the (1/4)° and (1/12)° data sets, the runoff volume is identical. To preserve in SPG12 the same atmospheric conditions present in Control, the CGRF data set is interpolated to (1/12)°, as opposed to using a higher-resolution data set. It should be noted that this does not imply true (1/12)° resolution of atmospheric forcing, as CGRF has a native resolution of around 33 km in the Labrador Sea. CGRF has, however, sufficient temporal and spatial resolution to capture the intense midlatitude cyclones, which heavily influence the Labrador Sea (Holdsworth & Myers, 2015). While a higher-resolution atmospheric data set might present some smaller scale features, the large-scale interaction between the atmosphere and the Labrador Sea will not change if the mean state is not significantly affected. The SPG12 simulation examines if additional eddy-resolving skill results with changes to the Labrador Sea subduction rather than the connection with the atmosphere (or Greenland melt), which the other simulations cover.

By implementing the nest, the horizontal resolution over the Labrador Sea increased from 16 km in Control to 5 km in SPG12. Due to the increased resolution, the following resolution-dependent parameters are consequently different between Control and SPG12: time step, horizontal eddy diffusion, horizontal bilaplacian eddy viscosity, and elastic wave time scale for sea ice (Table 2). The rest of the parameters for each simulation were kept identical.

The second perturbation experiment, termed Greenland Melt Reduced (*GMR*), aims to determine the impact of freshwater fluxes from the GrIS on LSW formation. Compared to the Control run, the simulation GMR does not include the GrIS freshwater around Greenland from Bamber et al. (2012). The difference in LSW formation between the two Control and GMR simulations is presented in section 4.2.

**Table 2**
*Resolution-Dependent Parameters Whose Numerical Values Changed From Control to SPG12*

| Parameter | *Control* | *SPG12* |
|---|---|---|
| Time step | 1,080 s | 180 s |
| Horizontal eddy diffusivity | 300 $m^2/s$ | 50 $m^2/s$ |
| Background horizontal bi-Laplacian eddy viscosity | $-1.5 \times 10^{11}$ $m^4/s$ | $-1 \times 10^{10}$ $m^4/s$ |
| Time scale for elastic waves in sea ice model | 320 s | 120 s |

To investigate the influence of high-frequency atmospheric forcing, a third perturbation experiment called Filtered was carried out. As high-frequency atmospheric phenomena appear as short time scale changes in temperature and wind stress, the temperature and wind speed fields only were filtered. To do so, a Kolmogorov-Zurbenko filtering (Rao et al., 1994; Zurbenko et al., 1996) was applied to the hourly atmospheric forcing data (referred to as **CGRF** (••) in Table 1). The filter is based on an iterative moving average of length $m$, and obtained after $p$ iterations, that removes high-frequency (with respect to the window size $m$) variations from the original data. We used a window length width of 10 days ($m = 10$) and one iteration ($p = 1$). Thus, all the forcing acting over a time period of 10 days or less (e.g., storms, barrier, and topographic winds and frontal jets) were removed from the original atmospheric forcing data set.

To analyze just the impact of the freshwater input as a consequence of changes in precipitation, a fourth perturbation experiment called Precipitation Decreased (*PD*) is considered. The precipitation used in the PD simulation is one third of that used in Control (referred to as **CGRF (•)** in Table 1). The Control simulation is thus considered to be a case of increased precipitation here.

To account for the model adjustment from GLORYS2V3, we use only the output corresponding to the period 1 January 2004 to 31 December 2016. By analyzing some of the ocean fields from the model output, we found that, although short, this 2-year adjustment period is sufficient for the model to develop realistic interannual variability in the Labrador Sea, given the simulations start from the reanalysis solution.

### 2.3. Model Evaluation

We compared the mixed layer depth (MLD) obtained from Argo observations (for details about the Argo data set, see: Holte et al., 2017) with the Control simulation (based on the analysis of Courtois et al., 2017). The comparison was made over a region in the Labrador Sea selected following Yashayaev and Loder (2016; Figure 2c). The MLD from Control shows a good agreement with that derived from the Argo floats, especially during years when deep convection developed such as 2008, 2012, 2014, and 2015. Seasonal variability captured in the Control simulation corresponds well with that observed. The observed and simulated MLD time series are correlated at 81% for both periods 2002–2016 and 2004–2016. Thus, there is no impact whether we consider or not the short spin-up time. At the same time there is some disagreement as Control shows a deeper (more than 300 m) MLD in years like 2009, 2010, and 2016. However, due to the nature of the Argo floats, they do not happen to be always in the convection site when deep convection is occurring, as they mainly drift within the mean flow. Based on observational data (annual conductivity-temperature-depth survey of the AR7 W section from Fisheries and Oceans Canada), Yashayaev and Loder (2017) found that the MLD during 2016 was deeper than 2,000 m; however, the Argo data do not reach that depth. Thus, the differences found in the MLD comparison in the years 2009, 2010, and 2016 might as well come from the absence of observations from the convection region and not necessarily due to an overestimation of the model MLD.

We also compared over the MLD averaged salinity and temperature time series from Control and from Argo floats (for details about the Argo data set see Holte et al., 2017; Figures 2d and 2e, respectively), both within the same region used for the MLD comparison. We found that (although not perfect) the model does a decent job representing the interannual variability and magnitudes of both fields, especially for temperature. This is reflected in the agreement between model and observations during the convection (winter) season. The mean model-observations temperature difference is 0.2 and 0.3 °C for the periods 2002–2016 and 2004–2016, respectively. In the case of salinity the mean model-observations difference is 0.1 and 0.2 for the periods 2002–2016 and 2004–2016, respectively. We found that the modeled and observed salinity time series are 69% and 74% correlated for the periods 2002–2016 and 2004–2016, respectively. At the same time in the case of the temperature field, the model and observation time series are 95% correlated for both periods 2002–2016 and 2004–2016.

The overturning transport at 26.5°N between Control and the observations from the RAPID-MOCHA-WBTS (RAPID-Meridional Overturning Circulation and Heatflux Array-Western Boundary Time Series) array (Smeed et al., 2017), was also compared (Figure 2f). In this particular case the comparison is done from 2004, which is when the observations at the RAPID-MOCHA-WBTS array started. Both time series are correlated at 50% with the model properly representing the interannual variability. However, the model overestimates the overturning transport by 2 Sv with the difference increasing with time. The increase in the modeled AMOC at 26.5°N after 2009 seems to be related to numerical issues at the southern boundary (−20°S) beginning in December 2007. The signal, however, does not spread beyond 45°N during our integration and thus does not affect the Labrador Sea fields discussed in this manuscript.

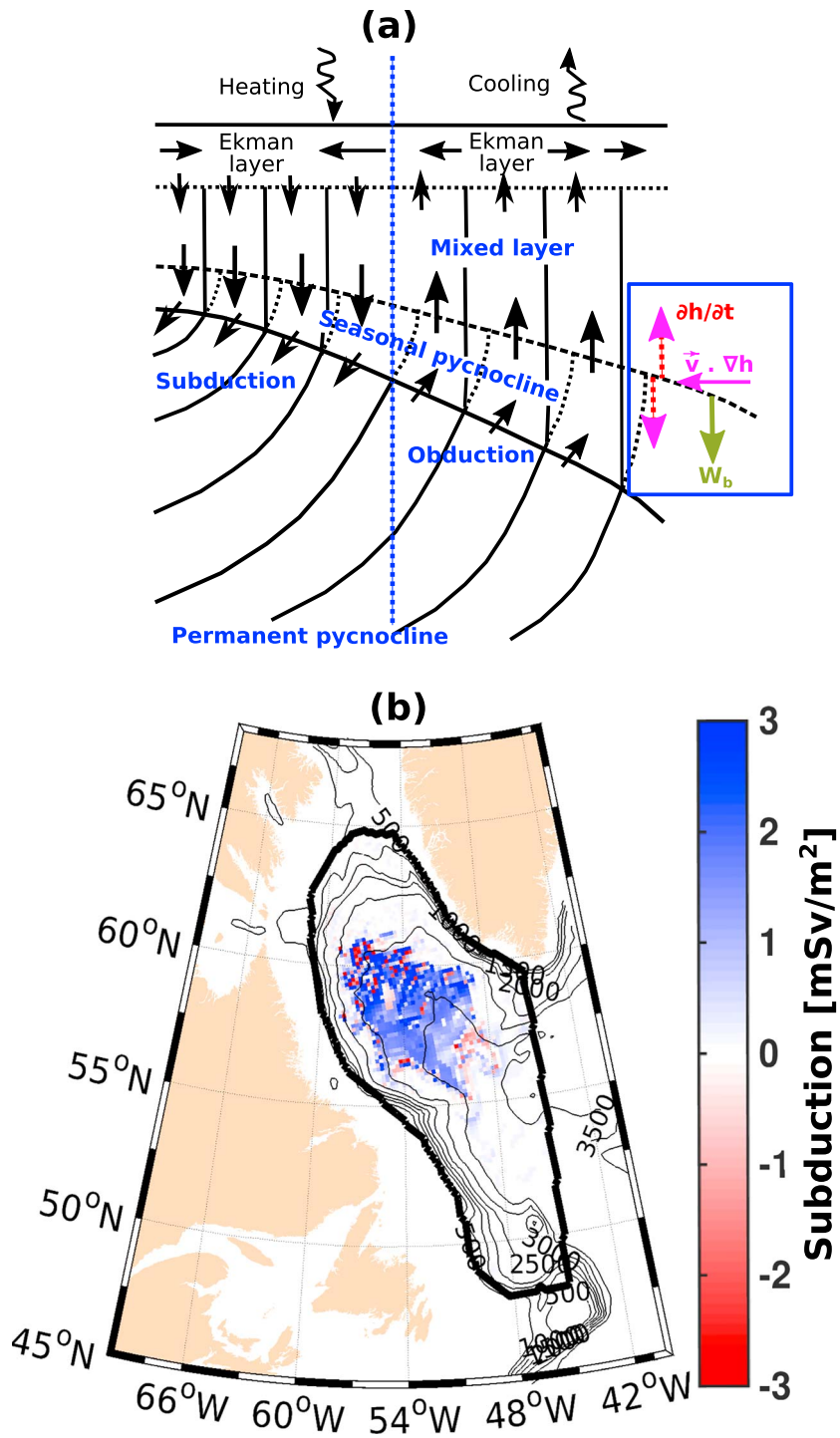


**Figure 3.** (a) Schematic showing the subduction and obduction process following Qiu and Huang (1995). The blue box represents the processes involved in subduction. The red arrows represent the change in time of the mixed layer depth (MLD), with the arrows pointing out the shallowing (up) and deepening (down) of the MLD ($\frac{\partial h}{\partial t}$). In magenta is illustrated the term that represents the convergence of horizontal transport into the MLD ($\vec{v} \cdot \nabla h$). In green appears the vertical transport of fluid ($W_b$) into the MLD. (b) The Labrador Sea with the region within the basin over which the net subduction was calculated. (b) A sample field of the subduction averaged over 26 (included) to 30 April 2012. It is chosen to illustrate a strong subduction period.

Müller et al. (2017) compared the mean circulation patterns from Control and SPG12 with that from satellite altimetry, with a focus on the region located between 60° to 5°W and 40° to 55°N within the subpolar gyre, finding a good correspondence between them. However, they did point out, as one of the differences, a more pronounced coastal branch of the LC represented in the simulations compared to that from altimetry data.

## 3. Analysis Methods

Ocean subduction involves water mass exchange through the moving ML base. When water masses are transferred beneath the base of ML, they are shielded from the atmosphere and only subsequently modify their properties by mixing in the ocean interior. The process describing the temporary movement of water out of (into) the ML is known as detrainment (entrainment; (see, e.g., Da Costa et al., 2005). On the other hand, when the water leaves the ML, passing through the seasonal pycnocline to the permanent pycnocline (Figure 3a) irreversibly in 1 year, it is known as subduction (e.g., Qiu & Huang, 1995). Similarly, the annual mean obduction rate is defined as the total amount of water going from the permanent pycnocline, passing through the seasonal pycnocline, into the ML (Figure 3a) irreversibly in 1 year (e.g., Qiu & Huang, 1995). We will use only the term subduction as it is the process linked to water formation, while obduction is mainly related to water erosion (e.g., Huang, 2010; Qiu & Huang, 1995).

Two main approaches can be used for calculating subduction rates. One approach is based on the analysis of ocean-atmosphere heat and mass fluxes and on the calculation of the density fluxes through the sea-air interface (Speer & Tziperman, 1992). The second approach is the so-called kinematic method, which is based on the analysis of the upper ocean circulation, and it can be carried out in a Lagrangian or Eulerian reference frame (e.g., Qiu & Huang, 1995). In the present work the kinematic subduction approach in Eulerian coordinates, following Da Costa et al. (2005) and Courtois et al. (personal communication, 2018), is used to calculate the subduction rate in the Labrador Sea (Figure 3b). According to Da Costa et al. (2005), the approach addresses the subduction rate as the exchange through the moving ML caused by a deepening (shallowing) of the MLD, convergence of horizontal transport out of (into) the ML and vertical transport out of (into) the ML (Figure 3a). So all the processes contributing to the transfer of water into the ocean interior are considered.

Following the discussion in Da Costa et al. (2005) and Courtois et al. (personal communication, 2018), the subduction rate $S$ is defined as follows:

$$S(\sigma) = \frac{-1}{\tau}\int_0^{\tau}\int_{A_\sigma}[W_b + \frac{\partial h}{\partial t} + \vec{v}\cdot\nabla h]\,\mathrm{d}A_\sigma\,\mathrm{d}t, \tag{1}$$

where $S(\sigma)$ is the net subduction, $\tau$ is 1 year, and $\mathrm{d}A_\sigma$ is the element surface outcrop area associated with $A_\sigma = [x : \sigma \leq \sigma_h(x,t) < \sigma + \delta\sigma]$ with $\sigma_h$ the instantaneous ML density, $\mathbf{x} \equiv (x,y)$ are the horizontal coordinates, $t$ is time, $h$ is the MLD, $v$ is the velocity, and $\sigma$ and $(\sigma + \delta\sigma)$ represent the density of neighboring isopycnals. A major advantage of this method is that it considers the three main ways in which a parcel of water can leave or enter the ML: $W_b$ represents the vertical velocity at the base of the ML, $\frac{\partial h}{\partial t}$ represents the changes in time of the ML thickness and $(\vec{v}\cdot\nabla h)$ the horizontal advection across the sloping base of the ML.

$W_b$ is not extracted directly from the model output but instead is computed according to Huang (2010) where

$$W_b = W_e - \frac{\beta}{f}\int_{-h}^{0} v\,\mathrm{d}z. \tag{2}$$

Following Huang (2010), $W_b$ is the contribution to the net subduction due to vertical pumping at the base of the ML, which is slightly smaller than the Ekman pumping rate ($W_e$) due to the geostrophic flow ($\frac{\beta}{f}\int_{-h}^{0} v\,\mathrm{d}z$) in the ML. Accordingly, $W_e$ is computed as the divergence between the meridional ($\tau^y$) and zonal ($\tau^x$) wind stress, both given by the atmospheric forcing. The second term in equation (2), $\frac{\beta}{f}\int_{-h}^{0} v\,\mathrm{d}z$, is computed by integrating $v$ over the ML. $\beta = \frac{\partial f}{\partial y}$ and $f$ is the Coriolis parameter.

Two density classes were considered for computing the subduction rate. Following Stramma et al. (2004), Kieke et al. (2006) defined Upper Labrador Sea Water (ULSW) and deeper LSW to fall into the density range $\sigma_\theta = 27.68$–$27.74$ kg/m$^3$ and $\sigma_\theta = 27.74$–$27.80$ kg/m$^3$, respectively. In this paper, following both studies we define ULSW in the same density range. In the case of deeper LSW we define it as a water mass in the density range $\sigma_\theta = 27.74$–$27.82$ kg/m$^3$. Numerical simulation salinity drift in this region is a known problem

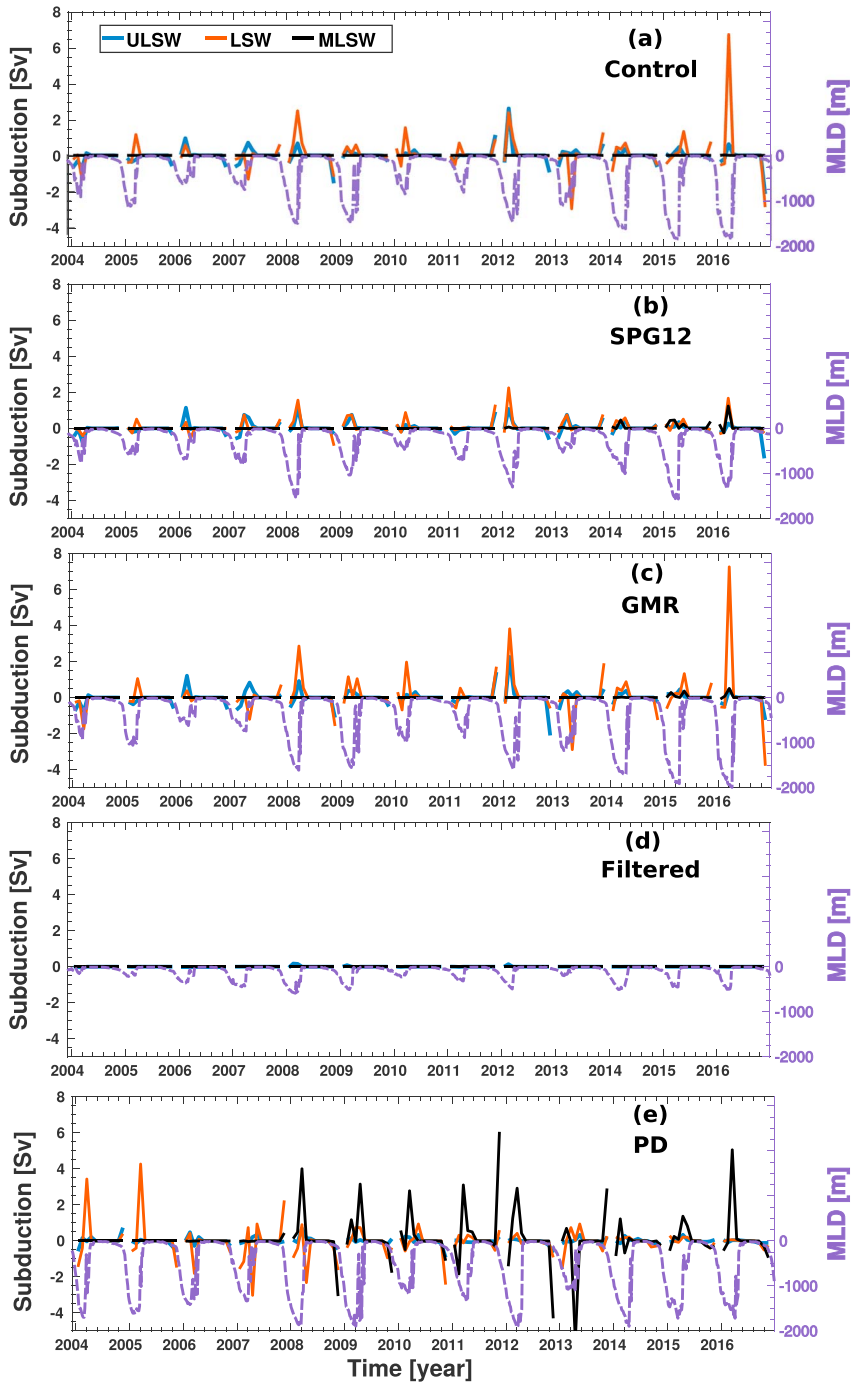


**Figure 4.** Monthly subduction and obduction rates (in Sverdrup), from January 2004 to December 2016, considering the density ranges of ULSW (Class1: blue), deeper LSW (Class 2: orange), and model LSW (Class 3: black). Shown are the simulations: (a) *Control*, (b) *SPG12*, (c) *GMR*, (d) *Filtered*, and (e) *PD*. Maximum model MLD (dashed purple lines) for each simulation appears overlaid on the subduction time series. GMR = Greenland Melt Removed; LSW = Labrador Sea Water; MLD = mixed layer depth; MLSW = Modelled Labrador Sea Water; PD = Precipitation Decreased; ULSW = Upper Labrador Sea Water.

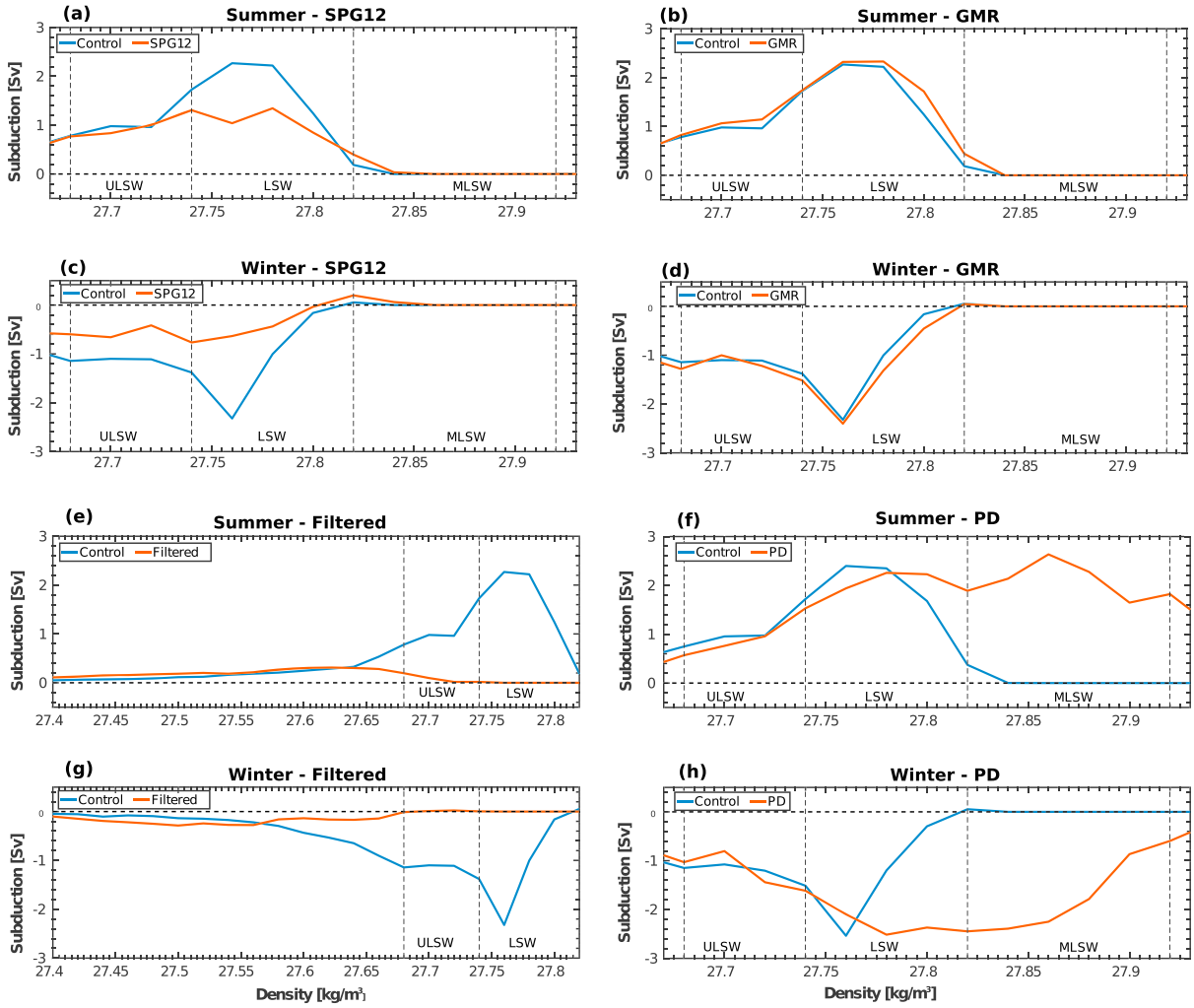


**Figure 5.** Averaged seasonal subduction and obduction rates as a function of the potential density, for each of the perturbation experiments compared to *Control*: (a, c) *SPG12*, (b, d) *GMR*, (e, g) *Filtered*, and (f, h) *PD*. In all the cases the Control simulation appears in blue, while the perturbation (depending on the experiment) appears in orange. The summer season is defined as the period from April to September, while the winter season goes from October to March. GMR = Greenland Melt Removed; LSW = Labrador Sea Water; MLSW = Modelled Labrador Sea Water; PD = Precipitation Decreased; ULSW = Upper Labrador Sea Water.

(e.g., Rattan et al., 2010). Thus, simulated density tends to increase as the time evolves. For this reason an additional water mass is considered: A water mass with a fixed density ranges from $\sigma_\theta = 27.82$–$27.92$ kg/m$^3$, which will be referenced as Modelled Labrador Sea Water (MLSW). However, not all the simulations show subduction occurring within such density range. In fact, the Control simulation shows no subduction occurring at the MLSW density range.

By default in NEMO, the MLD is calculated using a density difference criterion of 0.01 kg/m$^3$. As explained in Courtois et al. (2017), the MLD computed this way is overestimated during strong deep convection events due to temperature-salinity compensation. Given the dependence of the kinematic approach on the MLD, we defined and computed MLD as explained in Courtois et al. (2017; Figure 2c for Control-MLD). Therein, the MLD is estimated based on the intersection of two linear fittings, one defined by the ML and the other one by the slope of the underneath layer, for both potential temperature and salinity.

## 4. Results

In this section we will describe the results from the different perturbation experiments. The order of presentation will be as follows: SPG12, GMR, Filtered, and finally PD. For each of the experiments the

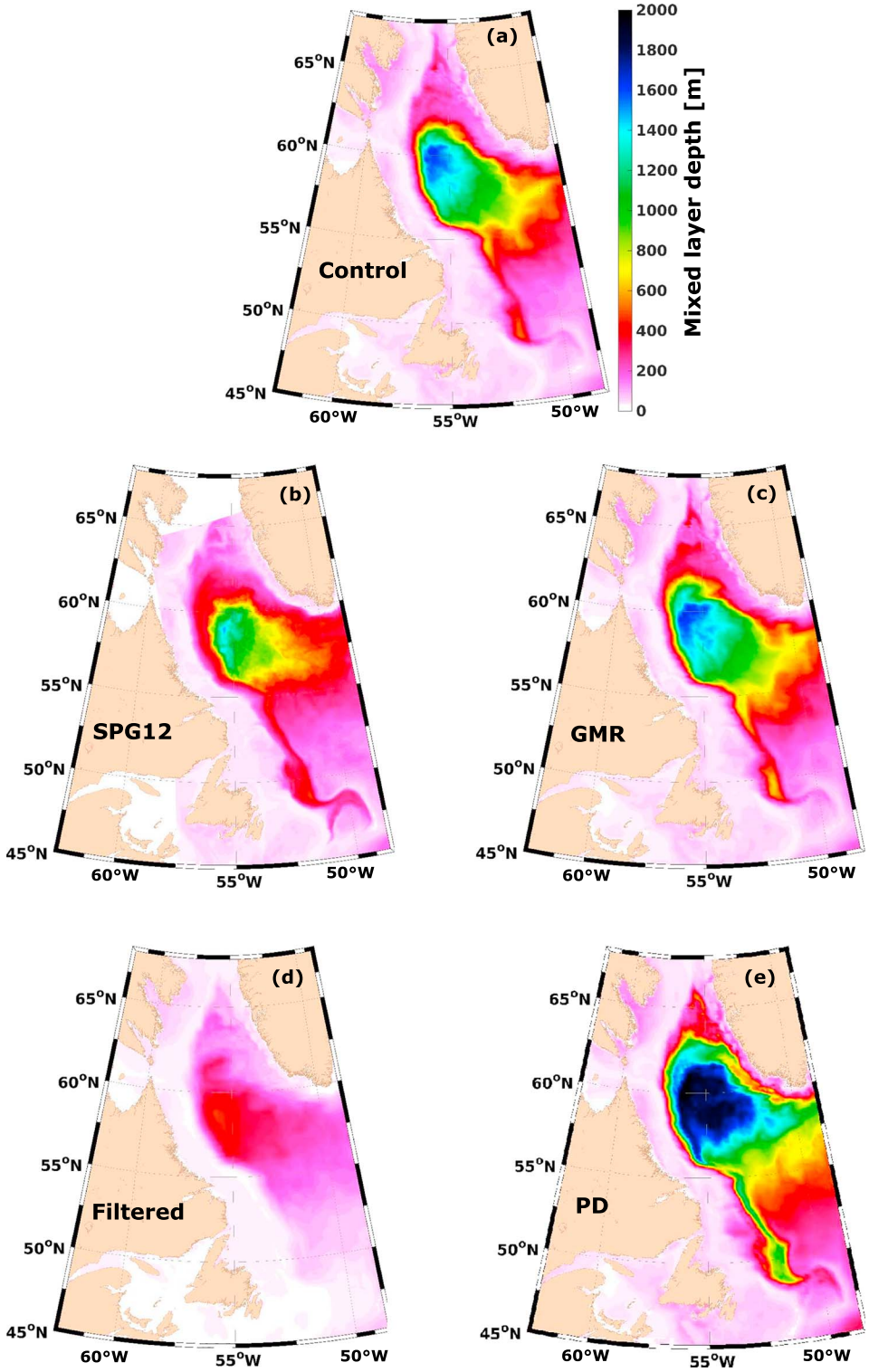


**Figure 6.** March mixed layer depths in the Labrador Sea, averaged over the years 2004 to 2016, for (a) *Control*, (b) *SPG12*, (c) *GMR*, (d) *Filtered*, and (e) *PD*. For SPG12 (b) no mixed layer depth values are shown outside the high-resolution nest (region in white). GMR = Greenland Melt Removed; PD = Precipitation Decreased.

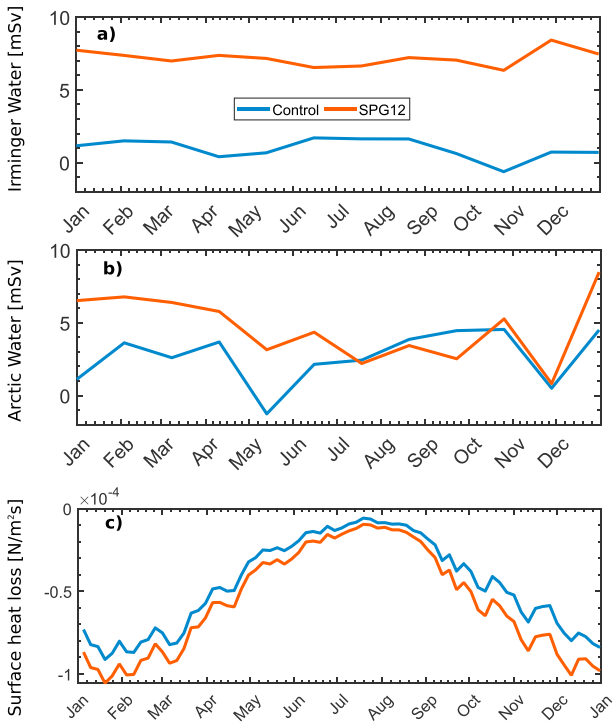


**Figure 7.** Climatology of (a) Irminger Water and (b) Arctic Water spawned out of the West Greenland Current into the study region in the Labrador Sea (Figure 3b), for *Control* and *SPG12*. Arctic Water is defined as water fresher than 34.8 and lighter than $\sigma_\theta$=27.68 kg/m$^3$. Irminger Water is defined as a water mass saltier than 34.8 and lighter than $\sigma_\theta$=27.68 kg/m$^3$ (our potential density minimum for Upper Labrador Sea Water). Panel (c) shows the climatology for the thermal forcing component of the buoyancy fluxes for *Control* and *SPG12* (heat loss only in this case), in the same region as in (a) and (b).

monthly mean subduction, seasonal mean subduction, averaged March MLD, mean total subduction, and the averaged subduction components will be described for the period 2004–2016.

### 4.1. Changing the Horizontal Resolution (SPG12 Experiment)

Monthly averaged subduction time series together with the maximum model MLD were plotted to investigate the evolution of the subduction during the study period and its relation with the MLD (Figure 4). It is worth noting that the time series in Figure 4 appear to be interrupted, most of the time at the beginning of each year. This occurs when entrainment and detrainment cancel each other resulting in no net subduction. In any case, the seasonality of the subduction is well represented. As the MLD deepens the water that once was beneath the ML enters it and gets mixed with the ambient waters and thus ventilated. This process is followed by the subduction (positive values), in late winter or early spring (late March to the end of April), as the MLD starts to shallow from its late winter maximum (Holte & Straneo, 2017). Under these circumstances the water within the ML leaves it and gets again trapped underneath its base.

In Control (Figure 4a) the subduction values are between 0.2 and 6.5 Sv. Three maxima occur: the first one (~2.5 Sv) in 2008 in the density class of deeper LSW (1 Sv at the ULSW density class); the second one in 2012, in this case in both density classes, ULSW and deeper LSW, with values of ~2.6 Sv and ~2.5 Sv, respectively, and the third one in 2016, with the subduction rate reaching 6.5 Sv in the density class of deeper LSW (and 0.5 Sv at ULSW). These years (2008, 2012, and 2016) coincide with observations of strong convection in the Labrador Sea (Yashayaev & Loder, 2017). During the years 2014 and 2015 the subduction was not as pronounced as during 2012 even though they were years of strong convection. However, strong convection does not mean that subduction will occur. Convection can broadly be described as a strong mixing of the water column involving downward and upward movement of fluid within the MLD, while subduction refers only to the net downward movement of fluid beneath the MLD. Nevertheless, during these years LSW was most likely building up, resulting in 6.5 Sv of deeper LSW being subducted in 2016.

In SPG12 (Figure 4b) the values of subduction are in general smaller than those in Control. The annual evolution of subduction in SPG12 also shows three noticeable maxima. As in Control, the first one occurs in 2008 at the density class of deeper LSW, with a value of 1.52 Sv and 1 Sv at ULSW. The second one in 2012, with 2.5 Sv at deeper LSW, and 1 Sv at ULSW. The third one occurs in 2016 with a subduction rate of 1.75 Sv at the deeper LSW and 0.25 Sv at ULSW.

In SPG12 from 2014 onward some subduction occurs at the density range of MLSW. Comparing the values of subduction for the deeper LSW class in SPG12 with those from Control, we find that, for SPG12 in 2008 the subduction rate decreases by 39%, no differences are shown in 2012, while in 2016 it decreases by 73%. As for the ULSW in SPG12, no differences are found in 2008, and it decreases by 62% and 50% in 2012 and 2016, respectively.

A seasonal decomposition of subduction for the SPG12 and Control allows a closer inspection of the process by density ranges (Figures 5a and 5c). The subduction rates (positive) were averaged over two different periods: The restratification period (summer), from the beginning of April to the end of September, and the period when the ML is deepening from the beginning of October to the end of following-year March, from 2004 to 2016. Both simulations show subduction occurring in the summer period (Figure 5a), which is when the MLD shallows and water gets transferred below the MLD base. In Control (Figure 5a, blue line) the subduction goes up to a maximum of ~2.3 Sv, while for SPG12 the maximum is around ~1.2 Sv. Both the summer and winter subduction decrease with increased resolution. Both maxima occur at the density range corresponding to deeper LSW. On average, when the resolution is increased over the subpolar gyre, the seasonal subduction rate in the Labrador Sea decreases by around 48%.

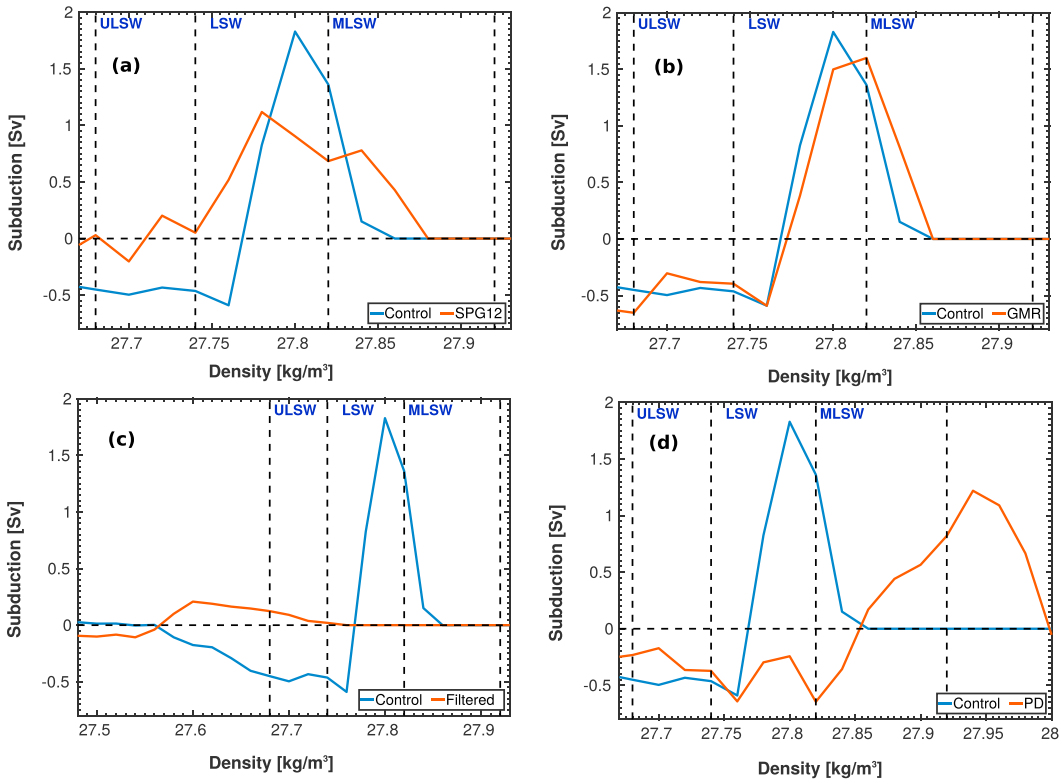


**Figure 8.** Mean total subduction rate as a function of the potential density. The average was done over the period 2004–2016 and for all the experiments. Each panel compares the *Control* simulations with is perturbations: (a) *SPG12*, (b) *GMR*, (c) *Filtered*, and (d) *PD*. For each case Control appears in blues, while the rest of the simulations, depending on the experiment, appears in orange. Notice that the *x* axis in (c) and (d) are different in order to better represent the maximum subduction rate in Filtered and PD, respectively. GMR = Greenland Melt Removed; LSW = Labrador Sea Water; MLSW = Modelled Labrador Sea Water; PD = Precipitation Decreased; ULSW = Upper Labrador Sea Water.

Even when the subduction is more prominent during the summer period, there is some subduction occurring in the winter period (Figure 5c). This is more pronounced in the SPG12 simulation where the subduction reaches 0.2 Sv at the interface between ULSW and deeper LSW density classes. In the case of the Control simulation (Figure 5c), the subduction does not even reach 0.1 Sv. The difference in the subduction magnitude found between Control and SPG12 can be explained by considering how the MLD varies from one simulation to the other. Figures 6a and 6b show the March averaged MLD over the Labrador Sea, from 2004 to 2016, for Control and SPG12, respectively. By increasing the spatial resolution not just the maximum depth of the ML decreases by around 17% but also the area where the ML is deeper than 1,000 m is reduced.

This could indicate an increase, due to increasing the resolution, in IR and BCE, which would transport IW into the Labrador Sea interior. IR have warm and saline IW cores between 200 and 1,000 m and low-salinity cores above 200 m. Indeed, Figure 7 shows higher transport of IW (Figure 7a) and freshwater (Figure 7b) from the WGC directly into our study region, in SPG12 compared to Control. A larger thermal forcing component (heat loss only in this case) of the buoyancy fluxes (Figure 7c) in SPG12 especially in fall and winter appears to follow the larger advection of IW in this simulation compared to Control.

Given their cold and fresh caps, mostly observed during spring (and also captured in SPG12: Figure 7b), IR are known to be an important source of freshwater to the Labrador Sea contributing significantly to the rapid restratification of basin interior following wintertime deep convection (de Jong et al., 2014; Gelderloos et al., 2011; Hátún et al., 2007). Hátún et al. (2007) observed and described IR spawned from the WGC as they entered the Labrador Sea interior by using high-resolution autonomous Seaglider hydrography and satellite altimetry. They suggested that the trajectory followed by these eddies keeps the observed region of deep convection to be small and not spatially the same as where the atmospheric wintertime cooling is most intense. This would explain the smaller convection region found in SPG12 compared to Control. BCE and CE are also known to play an important role in extracting heat from the boundary current system and

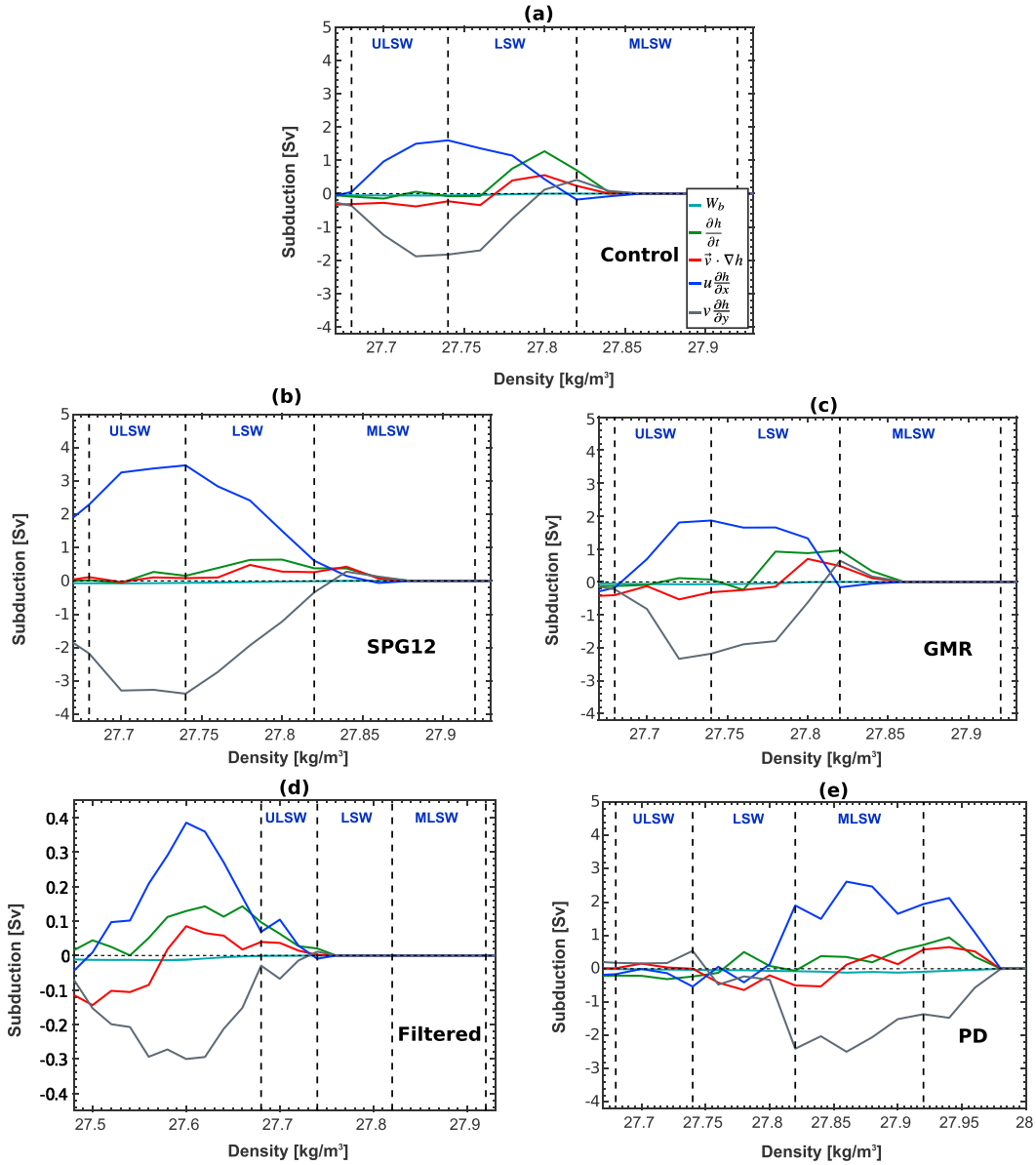


**Figure 9.** Time-averaged subduction components (equation (1)) as a function of the potential density. The average was done over the period 2004–2016 and for all the simulations: (a) *Control*, (b) *SPG12*, (c) *GMR*, (d) *Filtered*, and (e) *PD*. Vertical velocity ($W_b$) is represented in teal, the change in time of the mixed layer depth ($\frac{\partial h}{\partial t}$) appears in green, components of the horizontal advection, $u\frac{\partial h}{\partial x}$ and $v\frac{\partial h}{\partial y}$, appear in blue and gray respectively, and the resultant horizontal advective term $\vec{v} \cdot \nabla h$ is represented in red. Please notice that for the cases of (d) and (e), Filtered and PD respectively, the $x$ and $y$ axes are different compared to the other panels. This was done in order to better show the details of the components in each of the simulations. GMR = Greenland Melt Removed; LSW = Labrador Sea Water; MLSW = Modelled Labrador Sea Water; PD = Precipitation Decreased; ULSW = Upper Labrador Sea Water.

transport it to the interior of the basin (Chanut et al., 2008). During deep convection all three types of eddies would strengthen the stratification throughout the water column, shallowing the MLD and limiting the LSW production. As the subduction calculations are highly dependent on the MLD, seasonal changes in the MLD are also reflected in the seasonality of the subduction.

Figure 8a compares the mean total subduction rate as a function of the potential density for SPG12 with respect to Control, from 2004 to 2016. Different from Figure 4, Figure 8 comprises both seasons that allow us to determine an annual formation rate. For both simulations the maximum subduction rate, with values of 1.85 and 1.1 Sv for Control and SPG12, respectively, occurs at the density class corresponding to the deeper

LSW. This represents a 19% decrease in the net mean subduction rate when the resolution increases. This decrease is explained by analyzing all the components that impact on the net subduction rate (equation (1)).

Figures 9a and 9b show the components of the net subduction rate (1) as a function of the potential density, averaged from 2004 to 2016, for Control and SPG12, respectively. The vertical component $W_b$ (teal) has almost no contribution to the net subduction in both simulations. A significant term in both simulations is $\frac{\partial h}{\partial t}$ (green), which represents the change in time of the MLD. For Control and SPG12 the term reaches a maximum value of 1.4 and 0.6 Sv, respectively, being 57% higher in Control. This is consistent with the average March MLD, which is deeper in Control. For both simulations $\frac{\partial h}{\partial t}$ is maximum at the density range of the deeper LSW.

The advective term $\vec{v} \cdot \nabla h$ (red) is larger (by 33%) at the density range of deeper LSW in Control relative to SPG12. In Control it reaches 0.6 Sv, while in SPG12 it reaches 0.4 Sv. However, the advective term in SPG12 is larger at the density ranges of ULSW and MLSW, resulting in subduction values of ≃0.25 and ≃0.75 Sv, respectively (Figure 8a). Meanwhile, in Control subduction at those density ranges is much smaller or nonexistent. Also, in SPG12 this term is positive for all three water masses defined, contributing to the subduction rate in every LSW layer, while it is not entirely positive in the Control simulation.

In Control, the subcomponents of $\vec{v} \cdot \nabla h$ do not reach their maximum values in the same density range. $u\frac{\partial h}{\partial x}$ (blue) reaches a maximum value of 1.6 Sv at the interface between ULSW and deeper LSW density classes, while $v\frac{\partial h}{\partial y}$ (gray) is maximum in the density range of ULSW, reaching −2 Sv. This explains why $\vec{v} \cdot \nabla h$ in Control is negative in the density range of ULSW, while it is predominantly positive in the density range of deeper LSW. In SPG12, $u\frac{\partial h}{\partial x}$ and $v\frac{\partial h}{\partial y}$ reach a maximum of 3.5 and −3.4 Sv, respectively.

### 4.2. Impact of Removing Greenland Freshwater Discharge (GMR Experiment)

The perturbation experiment GMR serves to analyze the impact of runoff from GrIS. As the simulation Control was described in the previous section, we will proceed here to describe GMR and address the differences or similarities between them. Monthly subduction for this experiment is shown in Figures 4a and 4c, for Control and GMR, respectively. In GMR the subduction values are in general larger in magnitude compared with the same events in Control. As in Control, maximum subduction occurs for GMR during 2008, 2012, and 2016. The subduction rate in 2008 reaches a magnitude of 3 Sv at the density class of deeper LSW and 1 Sv at the range corresponding to ULSW. This represents an increase in the subduction rate of 20% at the density class of deeper LSW, with no changes occurring for the subduction at ULSW.

For 2012 the subduction rate in GMR reaches values of 4.5 and 2.5 Sv in the density range of deeper LSW and ULSW, respectively. This means that in 2012 the subduction increases by 80% for deeper LSW and it decreases by 4% for ULSW, with respect to Control. In 2016, the subduction rate reaches 7.5 Sv at the density class of deeper LSW and 0.5 Sv at ULSW. This represents an increase (with respect to Control) in the subduction rate by 15% for deeper LSW, while no changes are found for ULSW. Without the presence of Greenland melt the LSW gets denser, with an increase in the formation of deeper LSW from 2008 to 2016. As in SPG12 there is some subduction occurring in GMR at the density range of MLSW after 2015.

The seasonality of the subduction for the GMR experiment is shown in Figures 5b and 5d. In the case of the summer subduction (Figure 5b), the maximum rate occurs in both simulations (GMR and Control) at the density of deeper LSW. The maximum rate for GMR is ∼2.4 Sv, which is 4.3% larger than the 2.3 Sv reached in Control. During the winter season (Figure 5d) both simulations show very little subduction occurring at the interface between deeper LSW and MLSW. The magnitude of the subduction in both cases is less than 0.1 Sv.

The averaged March MLD also responds to the presence or, in the case of the GMR experiment, the absence of Greenland melt. Comparing this simulation with Control, we find that the maximum MLD (in GMR) is ∼5% deeper than in Control (Figure 6c). In GMR the area where the MLD is deepest also increases compared with Control. This difference in the MLD is clearly reflected in the summer subduction (mainly over the deeper LSW density class), which increases by 4.3% when the freshwater fluxes from the GrIS are not considered.

The mean net subduction rate for GMR, averaged from 2004 to 2016, is represented in Figure 8b. While the maximum subduction in Control occurs in the deeper LSW density class, for GMR it occurs at the interface between deeper LSW and MLSW. This implies a density shift in the formation rate of LSW, being lighter

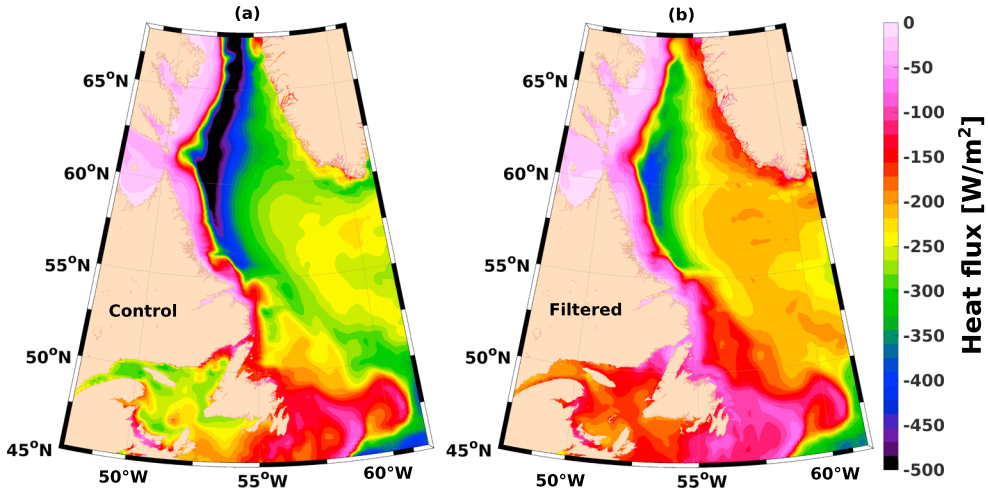


**Figure 10.** Averaged January heat flux (W/m$^2$) from 2004 to 2016 over the Labrador Sea, for (a) the *Control* and (b) the *Filtered* simulations.

in Control due to the influence of Greenland melt. Concerning the magnitude, there is a decrease in the subduction rate by 14% in GMR with respect to Control as the maximum subduction rate in GMR is ~1.6 Sv.

The components of the net subduction rate for GMR are shown in Figure 9c. As in Control, the vertical component $W_b$ (teal) in GMR has almost no contribution to the net subduction rate. The term $\frac{\partial h}{\partial t}$ (green) reaches 1 Sv (only 0.4 Sv smaller than Control) in the interface between deeper LSW and MLSW, denoting a shift in the density compared to Control. At the density of ULSW, $\frac{\partial h}{\partial t}$ is no larger than 0.2 Sv, while it is around 0.9 Sv at the density of deeper LSW.

The advective term $\vec{v} \cdot \nabla h$ (red) in GMR, just like in Control, reaches its maximum of 0.6 Sv at the density of deeper LSW. By decomposing $\vec{v} \cdot \nabla h$ into $u\frac{\partial h}{\partial x}$ (blue) and $v\frac{\partial h}{\partial y}$ (gray), we notice that although their maximum values are higher than those in Control, their resultant component, $\vec{v} \cdot \nabla h$, is effectively lower than in Control. This results from the fact that $v\frac{\partial h}{\partial y}$ is larger in magnitude (−2.4 Sv) than $u\frac{\partial h}{\partial x}$ (1.8 Sv), reaching both their maxima at the density of ULSW. This is also why we notice that $\vec{v} \cdot \nabla h$ is negative at the density of ULSW, becoming positive at the density of 27.785 kg/m$^3$.

### 4.3. Impact of High-Frequency Atmospheric Phenomena (Filtered Experiment)

The Filtered experiment shows the important role of high-frequency atmospheric phenomena in driving deep convection (e.g., Holdsworth & Myers, 2015). Monthly subduction for Filtered is shown in Figure 4d, where the lack of subduction in Filtered shows the importance of the high-frequency atmospheric phenomena. The maximum subduction in Filtered is ~0.18 Sv and occurs in 2008 at the density class corresponding to ULSW. This is 82% lower than that in Control. Besides 2008, there are only two other years where the subduction is different from 0: 2009 with a rate ~0.08 Sv and 2012 with a rate ~ 0.15 Sv, both at the density class of ULSW. Considering the same density class, the subduction in Filtered during the years 2009 and 2012 is 89% and 85% smaller than that in Control, respectively. No subduction events occur at the classes corresponding to deeper LSW and MLSW. So even when in some years the ML reached 500- to 700-m depth there is little or no LSW formation at all.

The summer subduction for Filtered (Figure 5e) reaches a maximum of ~0.4 Sv at 27.63 kg/m$^3$, this is even lighter than ULSW. Compared with Control, this is 83% smaller in magnitude. There is no contribution at the ranges of deeper LSW and MLSW. Furthermore, in the case of the winter season (Figure 5g), we find that no subduction occurs during this period. The maximum depth reached by the averaged March MLD for Filtered (Figure 6d) is no deeper than 500 m. This is, on average, 1,300 m (72%) shallower compared to Control. The mean total subduction rate (Figure 8c) also decreases with filtered atmospheric forcing. The maximum subduction rate for Filtered occurs at a density class lighter than ULSW (~27.6 kg/m$^3$) and is no greater than 0.2 Sv.

**Table 3**
*Magnitude of the Components in Equation (1) and Maximum 2004–2016 Mean Subduction Rate, for the Five Simulations Used in the Sensitivity Experiments*

| Simulation name | $\frac{\partial h}{\partial t}$ (Sv) | $\vec{v} \cdot \nabla h$ (Sv) | Maximum subduction rate (Sv) | Density of maximum subduction |
|---|---|---|---|---|
| *Control* | 1.4 | 0.6 | 1.85 | deeper LSW |
| *SPG12* | 0.6 | 0.4 | 1.1 | deeper LSW |
| *GMR* | 1 | 0.6 | 1.6 | 27.82 kg/m$^3$ |
| *Filtered* | 0.14 | 0.1 | 0.2 | 27.6 kg/m$^3$ |
| *PD* | 1 | 0.6 | 1.25 | 27.94 kg/m$^3$ |

*Note*. As there is almost no contribution from $W_b$ to the maximum subduction rate, it was excluded from the table.

Figure 9d shows the components of the net subduction for Filtered, averaged from 2004 to 2016. In order to have a better representation of the components in Filtered, the $y$ axis and the $x$ axis do not have the same magnitude range compared to Control. In Filtered the maximum values for all the components are concentrated in the density range between 27.5 and 27.68 kg/m$^3$, lighter than ULSW. Just as in Control, almost no contribution comes from $W_b$ (teal). The leading component is $\frac{\partial h}{\partial t}$ (green) and reaches 0.14 Sv. The advective term $\vec{v} \cdot \nabla h$ (red) is 0.08 Sv, 87% lower than in Control. By decomposing $\vec{v} \cdot \nabla h$ we see that both subcomponents reach their maximum values at ~27.6 kg/m$^3$. $u\frac{\partial h}{\partial x}$ (blue) is 0.38 Sv, while $v\frac{\partial h}{\partial y}$ reaches −0.3 Sv.

The shallow MLD and the low LSW formation rates appear to be a consequence of the 44% decrease in the oceanic heat loss in Filtered (Figure 10b) with respect to Control (Figure 10a). We present the month of January only as it is the one that shows the strongest heat loss in the Labrador Sea, thus a higher incidence of high-frequency atmospheric phenomena. However, the overall statement of a decrease in the heat loss in Filtered is also valid for the other months.

### 4.4. Impact of Decreased Precipitation (PD Experiment)

Here we compare the simulations Control and PD to explore the sensitivity of the LSW formation rate to precipitation changes. Monthly subduction rates for PD are shown in Figure 4e. Two noticeable maxima occur, one in 2012 with 6 Sv, and another in 2016 ~5 Sv. In both cases the subduction occurs at the density class of MLSW. In Control there is no subduction occurring at this density class. In PD after 2008 there is no more than 1 Sv of deeper LSW being subducted, while in the case of the ULSW this behavior is not seen since the beginning of the time series. This indicates a transformation of the LSW into the denser water mass MLSW.

The averaged summer subduction rate for PD (Figure 5f) reaches a maximum of 2.6 Sv in the density range of MLSW. In the density range of ULSW both simulations, Control and PD, show the same tendency as well as similar magnitudes. In the density range of deeper LSW PD reaches 2.2 Sv, 8% smaller than Control. There is no subduction occurring during the winter period (Figure 5h) for any of the water masses under study.

The average March MLD for the simulation PD (Figure 6e) also shows the impact of a decrease in the precipitation. The maximum MLD for PD increases by 20%. The spatial distribution of the deepest MLD (2,000 m) also increases in PD. Surprisingly, the net subduction does not show an increase (Figure 8d). Instead, the maximum subduction rate occurs at higher densities. Here, as in the GMR, the subduction rate decreases by 17% and shifts from 27.8 kg/m$^3$ (in Control) to 27.94 kg/m$^3$ (in PD). Nevertheless, in PD the effect is more dramatic, as in GMR the freshwater anomaly occurs only around Greenland while in PD it is over the entire ANHA domain.

The subduction components for PD are shown in Figure 9e. Compared to Control, the largest amplitudes of each of the terms are found at larger densities. The term $\frac{\partial h}{\partial t}$ has its maximum of 1 Sv at 27.85 kg/m$^3$. This is actually denser than MLSW and 29% decrease with respect to Control.

$\vec{v} \cdot \nabla h$, on the other hand, is maximum in the density of MLSW and it reaches 0.6 Sv, similar (in magnitude only) to Control. When decomposing $\vec{v} \cdot \nabla h$, we find that both components are maximum in the density of MLSW. $u\frac{\partial h}{\partial x}$ goes up to 2.6 Sv, while $v\frac{\partial h}{\partial y}$ reaches −2.8 Sv. Comparing them with the same terms in Control, we found that in PD the advective terms gain in magnitude but their resultant ($\vec{v} \cdot \nabla h$) is actually smaller

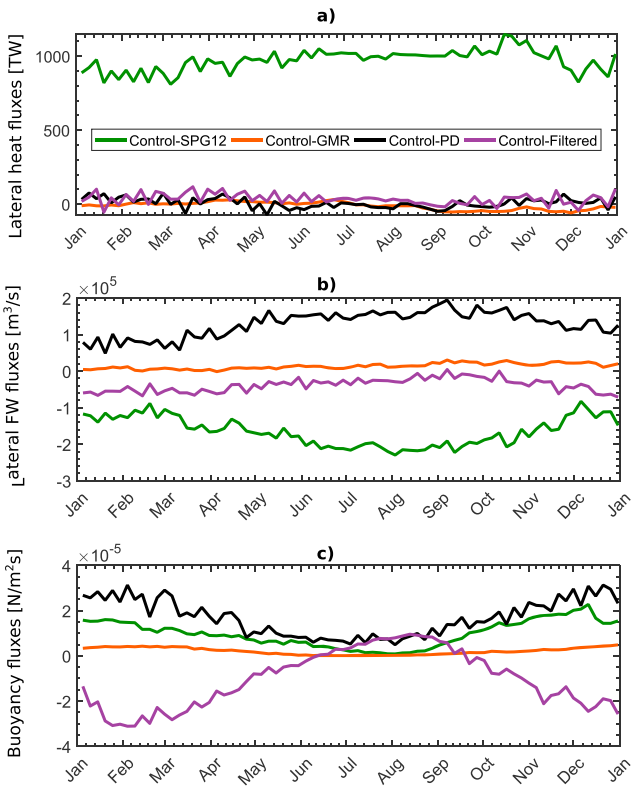


**Figure 11.** Climatological differences between *Control* and the perturbation experiments in the study region (black contour in Figure 3b), for lateral (a) heat and (b) freshwater fluxes and (c) buoyancy fluxes. Positive values indicate that the magnitude of the field is larger in Control and vice versa. GMR = Greenland Melt Removed; PD = Precipitation Decreased.

than in Control. The increase in the advective terms in PD is given by the increase in the horizontal density gradients.

## 5. Discussion and Conclusions

We have explored the sensitivity of subduction in the Labrador Sea to changes in spatial model resolution, Greenland freshwater discharge, high-frequency atmospheric forcing, and precipitation. A control and four perturbations experiments were implemented by using a coupled ocean-sea ice model, with an eddy-permitting regional configuration and an hourly atmospheric forcing. LSW formation rates were determined using a kinematic subduction approach. The study considered the period from 1 January 2004 to 31 December 2016.

Our Control simulation showed a maximum subduction rate of 1.85 Sv (Table 3) in the density class of deeper LSW (Figure 8a). Deep convection events that occurred during 2008, 2012, and 2016 (Yashayaev & Loder, 2017) were captured by Control (Figure 4a). During 2008, 1 and 2.5 Sv of ULSW and deeper LSW, respectively, were formed (Figure 4a). In the year 2012, 2.6 and 2.5 Sv of ULSW and deeper LSW, respectively, were formed (Figure 4a). The model convection event in 2016 resulted in formation rates of 0.5 and 6.5 Sv of ULSW and deeper LSW, respectively (Figure 4a). These numbers are within the range of previous studies; some of them are summarized in Figure 1b.

As part of a study on recurrent replacement of LSW, Yashayaev and Loder (2016) roughly estimated potential export rates of LSW. They did this by looking at winter to fall LSW disappearance rates, based on computing the area within the 550-m thickness contour of LSW. They indicated that their approach made a number of assumptions and likely overestimated the LSW export—which may or may not be directly tied to LSW production. Still, their analysis concluded that annual LSW export was 8.9 ± 1 Sv in strong convection year and 3.2 ± 1 Sv in weak convection years. Given more years of weak convection that strong convection over our study period (Yashayaev & Loder, 2016), our long-term mean estimate of 1.85 Sv in the density range of deeper LSW is not unreasonable. Furthermore, our largest formation rate, of 7 Sv (0.5-Sv ULSW and 6.5-Sv deeper LSW), in 2016, is not inconsistent with Yashayaev and Loder's (2016) estimate for strong convection years. We also note that Yashayaev and Loder (2017) point out that LSW newly formed in 2017 is the deepest, densest, and most voluminous since the mid-1990s.

We found that by increasing the resolution over the subpolar gyre, even when the advective terms produce more LSW, the LSW formation rate decreased in magnitude (Figure 8a). This was mostly due to shallower MLD and a decrease in the area of the deep convection in SPG12 compared to Control (Figures 6a and 6b).

During deep convection events, strong density differences between the convective region and the ambient stratified waters induce baroclinic instability which breaks up into CE (approximately diameter of 20–30 km). The CE mix the upper part of the water column, while the main part of the dense water sinks to its density level spreading later along isopycnals (see, e.g., Chanut et al., 2008; Lilly et al., 2003). These eddies together with BCE are thought to reduce the depth of the convective events (Jones & Marshall, 1993, 1997) as they are very effective at transporting heat and freshwater into the convective patch playing a major role in the early stages of restratification throughout the patch. Recently, Kawasaki and Hasumi (2014) explored in a modeling study the importance of eddy-induced near surface freshwater transport for inhibiting deep convection. They concluded that lateral buoyancy transport caused by heat is actually significantly larger than that from freshwater, with the later contributing mainly to the near the surface buoyancy transport only in the northern Labrador Sea. Their results, however, might be impacted by the absence of Greenland melt in their model. The freshwater advected into the Labrador Sea interior from the WGC mainly originated from the Arctic Ocean and runoff from the southeast GrIS (Gillard et al., 2016) and was transported south by the East Greenland Current. Failing to include Greenland melt in their model might explain

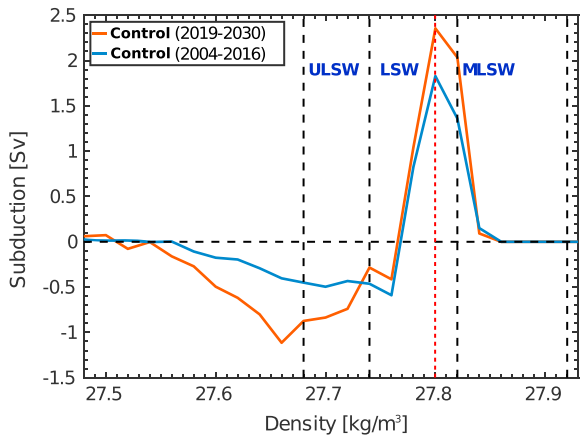


**Figure 12.** Mean total subduction rate as a function of the potential density for the *Control* simulation with different adjustment periods: 2004–2016 with 2 years of adjustment (blue) and 2019–2030 with 18 years of adjustment (orange). Red dashed line marks the density of the maximum subduction rate for both cases. LSW = Labrador Sea Water; MLSW = Modelled Labrador Sea Water; ULSW = Upper Labrador Sea Water.

why the upper 100-m freshwater thickness in their model is half of the observational estimates (Khatiwala et al., 2002).

Nevertheless, such processes potentially explain the averaged March MLD being shallower in SPG12 than in Control. There is actually more freshwater being advected into the study region in SPG12 (Figure 11b) possibly due to an increase in IR and BCE. This is not the case, however, for heat advection (Figure 11a), which is 3 orders of magnitude larger in Control. This leads to the buoyancy fluxes being larger, especially in winter and fall (Figure 11c), when (1/4)° is used.

The typical horizontal resolution of the numerical models used in the assessment reports of the Intergovernmental Panel on Climate Change is roughly 1° to 2° for the atmospheric component and around 1° for the ocean (Flato et al., 2013). Our results suggest that the use of ocean numerical models with coarse horizontal resolution results in LSW formation larger compared with estimates from numerical models with higher horizontal resolution. Thankfully, the upcoming CMIP6 (Overview of the Coupled Model Intercomparison Project Phase 6) will have (1/4)° for the ocean as the norm (Eyring et al., 2016). Nevertheless, the implications for coupled models are unproven and highly depend on atmosphere-ocean feedbacks, which are neglected in this study. At the same time different outcomes may result when high-resolution forcing fields (rather than interpolated low resolution fields) were considered.

We found that the presence of Greenland melt affects mainly the formation of denser LSW. The formation of LSW at a density of 27.82 kg/m$^3$ (in GMR), decreased by 14% when no Greenland melt is present, while there is more LSW been formed at a density of 27.8 kg/m$^3$ (Control) when freshwater fluxes from GrIS are considered (Figure 8b). However, our results indicate that the current trend in freshwater discharge from GrIS (Bamber et al., 2012) has not been followed by a decrease in the overall LSW formation rate. Also, the maximum MLD was not found to be greatly impacted by the presence of Greenland melt (Figures 4a and 4c). At the same time Control and GMR hold very little differences concerning lateral heat and freshwater and buoyancy fluxes (Figures 11a–11c)

In order to test if the integration time of the Greenland melt was actually an issue when looking at its influence on the LSW formation rate, the Control simulation was rerun from 2017 to 2030 using the same forcing that was used to run the period 2002 to 2016. Basically, the extended run (2017 to 2030) can be treated as a simulation over the period 2002 to 2016 but with a much longer adjustment. Figure 12 shows the formation rate for the two different periods: 2004 to 2016 and 2019 to 2030 (2004 to 2016 with a longer adjustment period) for the Control simulation. By increasing the adjustment period, the formation rate does not decrease, as might be expected as the Greenland melt water increases within the Labrador Sea. Instead, the LSW formation rate increases without changes in the density of the maximum subduction rate.

The use of a (1/4)° configuration might also be seen as a limitation for the GMR experiment given the poor representation of the eddy fluxes. By using the Parallel Ocean Program in two configurations, with horizontal resolutions of 1° and 0.1°, respectively, Weijer et al. (2012) explored the AMOC sensitivity to enhanced freshwater input from GrIS. They found that a reduction in wintertime convection (and the AMOC decline) is markedly more gradual and persistent in the 0.1° configuration. den Toom et al. (2014) used the same two configurations as in Weijer et al. (2012) to investigate the impact of the AMOC reduction on the freshwater advection in the North Atlantic. They also found a shallowing of the MLD in the Labrador Sea as a result of a 0.5-Sv freshwater perturbation from GrIS in the strongly eddying configuration. However, the freshwater fluxes from GrIS implemented in their experiments is “a worst-case scenario” compared to a “catastrophic collapse” of the GrIS (0.1 and 0.5 Sv). These simulations should not be considered as a realistic scenario for present-day climate change, which is the case of our study, where more realistic freshwater fluxes from the GrIS are considered. Böning et al. (2016) explored the impact of Greenland melt on deepwater formation in the North Atlantic Ocean by implementing a two-way nest over the polar/subpolar regions, increasing the resolution from (1/4)° to (1/20)° (VIKING20). As in our study, they used Bamber et al. (2012) to represent the freshwater fluxes from the GrIS. They found that the accumulation of freshwater from GrIS

so far has not been (yet) significant enough to impact the freshwater budget of the subpolar North Atlantic. In agreement with our results, they argued that the influence of meltwaters affects mainly the formation of the denser LSW. They pointed out that the dynamical implications given the decrease in the replenishment of the denser LSW might not be noticeable in less than a decade, in which case they might not emerge within the time frame of our study. The agreement between their findings and ours might make one think that a correct representation of freshwater fluxes from the GrIS is as important as the model horizontal resolution.

The experiment PD showed a similar behavior as the one from the GMR experiment. When a decrease in the precipitation was not considered (in Control), the LSW formed was effectively lighter, reaching a subduction maximum at 27.8 kg/m$^3$, while when the precipitation was reduced the subduction was maximum at 27.94 kg/m$^3$. This transformation was as a result of a decrease in freshwater advection and hence buoyancy fluxes in GMR over the study region (Figures 11b and 11c).

Our results suggest that an increased in the precipitation would impact mainly the replenishment of the denser LSW (Figure 8d). As in the GMR experiment, the increase in freshwater fluxes from precipitation did not impact greatly the maximum MLD in the Labrador Sea (Figure 4e)

Myers and Donnelly (2008) found an increase of $P - E$ (precipitation minus evaporation) in the mid-1970s. Similar to the freshening investigated here for the experiments GMR and PD, they suggest that the increase must have played some role in causing freshening in the Labrador Sea. Freshwater accumulation at the ocean surface is known to increase the water column stratification making it more difficult for deep convection to occur (Dickson et al., 1988). During the last five decades GrIS has undergone significant mass loss (Forsberg et al., 2017; Bamber et al., 2012; van Angelen et al., 2013; Velicogna et al., 2014) with the consequent enhanced contribution of freshwater to the ocean. Future precipitation increases as a result of an intensification of the global water cycle (Huntington, 2006; Wang et al., 2017) are one of the warming-induced hydrological changes. As temperature and water holding capacity of the atmosphere increases, so will the precipitation. This means that warmer climates will irreparably lead to more intense precipitation events (Wang et al., 2017), potentially impacting the winter deep convection in the Labrador Sea.

However, regardless of the warming-induced changes seen so far (e.g., Greenland melt increase), there has been a progressive deepening in the observed convection in the Labrador Sea since 2012, and $LSW_{2012-2016}$ is one of the deepest ever observed back to 1983 (Yashayaev & Loder, 2017). Our results show that, within the 12 years that our study spans, an increase in either precipitation or Greenland melt in the Labrador Sea is not likely to decrease the overall LSW formation rate or the maximum convection depth. It would, however, decrease the formation of denser LSW, which, by affecting the large-scale density gradients, would have longer-term dynamic implications. In fact, we could speculate that an increase in freshwater fluxes from the GrIS or an increase in midlatitude precipitation would likely impact the AMOC more by reducing the replenishment of denser LSW, than by decreasing the convection depth. These implications, however, cannot be further seen in our analysis as they are not likely to emerge within the 12 years of our study (Böning et al., 2016).

High-frequency atmospheric phenomena, like polar lows and cold-air outbreaks, are projected to decrease in the 21st century (Kolstad & Bracegirdle, 2008; Zahn & von Storch, 2010) also as consequence of global warming. These phenomena regulate the formation of deep water in the Labrador Sea by inducing a strong oceanic heat loss (Condron & Renfrew, 2013; Schulze et al., 2016), as they are accompanied by strong winds and a decrease in the air temperature (Kolstad & Bracegirdle, 2008; Zahn & von Storch, 2010). Yashayaev and Loder (2009) in their study argued that enhanced atmospheric cooling associated with below-normal air temperatures in the Labrador Sea was the predominant factor contributing to the enhanced production of $LSW_{2008}$. Våge et al. (2008) found this strong cooling to be related with (among other factors) a shift of the storms track more to the south compared to the previous winter, with the cyclones following a better well-defined trajectory from the east coast of North America toward the Irminger Sea. We found that by filtering out such events the heat loss over the Labrador Sea decreases by 44%. This reduction was enough to shut down the deep convection in the basin, with the March MLD not going deeper than 400 m. It took less than a year of filtered atmospheric forcing for the Filtered simulation to show a considerably decrease the LSW formation rate. It is important to note here that high-frequency atmospheric phenomena are projected to decrease based on relatively coarse resolution coupled models. How this result would change if high-resolution projections were available is still uncertain.

We understand that our Filtered simulation is an extreme scenario as basically all the storms are removed. In fact, if we translate the freshwater and heat fluxes of GMR and PD compared to those in Filtered into buoyancy fluxes, it becomes clear that the increase in Filtered is much larger (Figures 11a–11c). In terms of heat and buoyancy fluxes, the Filtered experiment could be compared with those in Weijer et al. (2012) where a worst-case scenario freshwater perturbation is applied, either around the perimeter of Greenland or over a broad swath (50–70°N) of the northern North Atlantic, using two model configurations at different resolutions. They found a reduction in ventilation in the Labrador Sea associated with a decrease in the ocean surface heat loss, all within the first few years. In both of their configurations, the decrease in the convective activity was reflected by a weakening of the AMOC within 10 years. Thus, our results point out that, global warming in the future by reducing the occurrence of storm events over the Labrador Sea and hence a decrease in the heat loss, is potentially as bigger threat for the LSW formation as an increase in the freshwater input. However, caution is required when drawing implications for a coupled system, where heat fluxes and sea surface temperature are not prescribed in the same way as in a forced numerical model simulation.

Holdsworth and Myers (2015) explored the impact of high-frequency atmospheric forcing in the convective energy on the Labrador Sea from 2002 to 2010 using model output. While convection represents vertical mixing (upward and downward), subduction focus only in the net downward transport of a specific water mass. A strong convection event (i.e., MLD deeper than 1,500 m) does not necessarily translate into an increase in the formation rate (Figure 4a). We found that deep convection events like those in 2014 and 2015 (Figure 4a) where the MLD was deeper than 1,500 m were not followed by an increase in the formation rate. We consider that, based on our results, care needs to be taken when directly linking convective energy to LSW formation. Different from Holdsworth and Myers (2015), we offer an estimate of the LSW formation rate when storms are not present. Our results not only support their findings but also extend their analysis and objectives. At the same time, the different diagnostic used in our study adds to our understanding of the link between LSW formation and convection.

We are aware that the presence of the artificial MLSW in the simulations SPG12, GMR, and PD (Figures 8b, 8c, and 8e) might be interpreted as if there is a significant influence from the model drift in our results. Böning et al. (2016) defined upper LSW between 27.74 and 27.82 kg/m$^3$, which is the density range we use here to define deeper LSW. At the same time they defined lower LSW between 27.82 and 27.92 kg/m$^3$, which is the density range that we use to define the MLSW. Attention needs to be paid when comparing LSW rates from different studies and their respective definitions in density ranges, and not just the names they were given. This does not mean that we are ignoring the presence of a small drift in our simulations. However, the Control simulation does not show the presence of subduction occurring in the density of MLSW, and it shows formation rates occurring at a density range comparable to observations (see, e.g., studies within Table 1). In the case of GMR and PD the transformation of ULSW and deeper LSW into MLSW is clearly due to the lack of Greenland melt and precipitation compared to Control, which induces an increase in the density, reflected in the deepening of the seasonal MLD.

The annual evolution of the subduction components in the case of SPG12 (not shown) links the transformation of ULSW and deeper LSW into the MLSW with an increase in the magnitude of the advective terms from 2014. When analyzing the velocity field from the model output in SPG12 (not shown), we found that there is an increase in the zonal velocities toward the east over the study region. The meridional velocities have a similar behavior, with an increase mainly toward the south. When using SPG12 to explore the temperature flux carried by individual eddies across 47°N in the Atlantic Ocean, Müller et al. (2017) compared its (SPG12) mean circulation patterns with satellite altimetry data, finding that the LC appeared to be more pronounced in SPG12. This might be a reason for the increase eastward and southward velocities found in our study region. Boundary issues between the parent domain and the nest might as well, eventually, lead to spurious solutions within the nest or child domain (Nash & Hartnett, 2014). Nevertheless, all the five simulations used were able to correctly capture the physical processes leading to LSW formation. At the same time the kinematic subduction approach has shown to be a useful tool when estimating LSW formation.

**Acknowledgments**
We gratefully acknowledge the financial and logistic support of grants from the Natural Sciences and Engineering Research Council (NSERC) of Canada. These include a Discovery Grant (rgpin227438-09) awarded to P. G. Myers, VITALS—RGPCC 433898, and an International Create (432295). We are grateful to the NEMO development team and the Drakkar project for providing the model and continuous guidance and to Westgrid and Compute Canada for computational resources. We would also like to thank G. Smith for the CGRF forcing fields, made available by Environment and Climate Change Canada. We thank Laura Castro de la Guardia for her aid in producing Figures 2c–2e. The Argo data used to create the climatological MLD and its properties were collected and made freely available by the International Argo Program and the national programs that contribute to it (http://www.argo.ucsd.edu and http://argo.jcommops.org). The Argo Program is part of the Global Ocean Observing System (http://doi.org/10.17882/42182). Data from the RAPID-WATCH MOC monitoring project are funded by the Natural Environment Research Council and are freely available from the website (http://www.rapid.ac.uk/rapidmoc). If interested in gain access to our model data, please contact P. G. Myers. D. Kieke acknowledges funding from the BMBF-RACE program. We also thank four anonymous reviewers for suggesting substantial improvements to the manuscript.

## References

Azetsu-Scott, K., Jones, E. P., Yashayaev, I., & Gershey, R. M. (2003). Time series study of CFC concentrations in the Labrador Sea during deep and shallow convection regimes (1991–2000). *Journal of Geophysical Research*, *108*(C11), 3354. https://doi.org/10.1029/2002JC001317

Bamber, J., van den Broeke, M., Ettema, J., Lenaerts, J., & Rignot, E. (2012). Recent large increases in freshwater fluxes from Greenland into the North Atlantic. *Geophysical Research Letters*, *39*, L19501. https://doi.org/10.1029/2012GL052552

Barnier, B., LeSommer, J., Molines, J. M., Penduff, T., Theetten, S., Treguier, A. M., et al. (2007). Eddy-permitting ocean circulation hindcasts of the past decades. *CLIVAR-Exchanges*, *12*(3), 8–10.

Blayo, E., & Debreu, L. (1999). Adaptive mesh refinement for finite-difference ocean models: First experiments. *Journal of Physical Oceanography*, *29*(6), 1239–1250. https://doi.org/10.1175/1520-0485(1999)029<1239:AMRFFD>2.0.CO;2

Böning, C. W., Behrens, E., Biastoch, A., Getzlaff, K., & Bamber, J. L. (2016). Emerging impact of Greenland meltwater on deepwater formation in the North Atlantic Ocean. *Nature Geoscience*, *9*(11), 523–527. https://doi.org/10.1038/ngeo2740

Böning, C., Bryan, F., Holland, W., & Döscher, R. (1996). Deep-water formation and meridional overturning in a high-resolution model of the North Atlantic. *Journal of Physical Oceanography*, *26*(7), 1142–1164. https://doi.org/10.1175/1520-0485(1996)026<1142:DWFAMO>2.0.CO;2

Brunnabend, S.-E., Schröter, J., Rietbroek, R., & Kusche, J. (2015). Regional sea level change in response to ice mass loss in Greenland, the West Antarctic and Alaska. *Journal of Geophysical Research: Oceans*, *120*, 7316–7328. https://doi.org/10.1002/2015JC011244

Chanut, J., Barnier, B., Large, W., Debreu, L., Penduff, T., Molines, J.-M., & Mathiot, P. (2008). Mesoscale eddies in the Labrador Sea and their contribution to convection and restratification. *Journal of Physical Oceanography*, *38*(8), 1617–1643. https://doi.org/10.1175/2008JPO3485.1

Condron, A., & Renfrew, I. A. (2013). The impact of polar mesoscale storms on northeast Atlantic Ocean circulation. *Nature Geoscience*, *6*(1), 34–37. https://doi.org/10.1038/ngeo1661

Courtois, P., Hu, X., Pennelly, C., Spence, P., & Myers, P. G. (2017). Mixed layer depth calculation in deep convection regions in ocean numerical models. *Ocean Modelling*, *120*, 60–78. https://doi.org/10.1016/j.ocemod.2017.10.007

Da Costa, M. V., Mercier, H., & Treguier, A. M. (2005). Effects of the mixed layer time variability on kinematic subduction rate diagnostics. *Journal of Physical Oceanography*, *35*(4), 427–443. https://doi.org/10.1175/JPO2693.1

Dai, A., Qian, T., Trenberth, K. E., & Milliman, J. D. (2009). Changes in continental freshwater discharge from 1948 to 2004. *Journal of Climate*, *22*(10), 2773–2792. https://doi.org/10.1175/2008JCLI2592.1

Dai, A., & Trenberth, K. E. (2002). Estimates of freshwater discharge from continents: Latitudinal and seasonal variations. *Journal of Hydrometeorology*, *3*(6), 660–687. https://doi.org/10.1175/1525-7541(2002)003<0660:EOFDFC>2.0.CO;2

de Jong, M. F., Bower, A. S., & Furey, H. H. (2014). Two years of observations of warm-core anticyclones in the Labrador Sea and their seasonal cycle in heat and salt stratification. *Journal of Physical Oceanography*, *44*(2), 427–444. https://doi.org/10.1175/JPO-D-13-070.1

Debreu, L., Vouland, C., & Blayo, E. (2008). AGRIF: Adaptive grid refinement in Fortran. *Computers & Geosciences*, *34*(1), 8–13. https://doi.org/10.1016/j.cageo.2007.01.009

den Toom, M., Dijkstra, H. A., Weijer, W., Hecht, M. W., Maltrud, M. E., & van Sebille, E. (2014). Response of a strongly eddying global ocean to North Atlantic freshwater perturbations. *Journal of Physical Oceanography*, *44*(2), 464–481. https://doi.org/10.1175/JPO-D-12-0155.1

Dickson, R., Lazier, J., Meincke, J., Rhines, P., & Swift, J. (1996). Long-term coordinated changes in the convective activity of the North Atlantic. *Progress in Oceanography*, *38*(3), 241–295. https://doi.org/10.1016/S0079-6611(97)00002-5

Dickson, R. R., Meincke, J., Malmberg, S.-A., & Lee, A. J. (1988). The "great salinity anomaly" in the northern North Atlantic 1968–1982. *Progress in Oceanography*, *20*(2), 103–151. https://doi.org/10.1016/0079-6611(88)90049-3

Dickson, R., Rudels, B., Dye, S., Karcher, M., Meincke, J., & Yashayaev, I. (2007). Current estimates of freshwater flux throught Arctic and subarctic seas. *Progress in Oceanography*, *73*(3), 210–230. https://doi.org/10.1016/j.pocean.2006.12.003

Dukhovskoy, D. S., Myers, P. G., Platov, G., Timmermans, M. L., Curry, B., Proshutinsky, A., et al. (2016). Greenland freshwater pathways in the sub-Arctic Seas from model experiments with passive tracers. *Journal of Geophysical Research: Oceans*, *121*, 877–907. https://doi.org/10.1002/2015JC011290

Eyring, V., Bony, S., Meehl, G. A., Senior, C. A., Stevens, B., Stouffer, R. J., & Taylor, K. E. (2016). Overview of the Coupled Model Intercomparison Project Phase 6 (CMIP6) experimental design and organization. *Geoscientific Model Development*, *9*(5), 1937–1958. https://doi.org/10.5194/gmd-9-1937-2016

Fichefet, T., & Maqueda, M. A. M. (1997). Sensitivity of a global sea ice model to the treatment of ice thermodynamics and dynamics. *Journal of Geophysical Research*, *102*(C6), 12,609–12,646. https://doi.org/10.1029/97JC00480

Flato, G., Marotzke, J., Abiodun, B., Braconnot, P., Chou, S., Collins, W., et al. (2013). Evaluation of climate models. In S. Solomon, D. Qin, M. Manning, Z. Chen, M. Marquis, B.-K. Averyt, et al. (Eds.), *Climate change 2013: The Physical Science Basis. Contribution of Working Group I to the Fifth Assessment Report of the Intergovernmental Panel on Climate Change*. Cambridge, United Kingdom and New York, NY, USA: Cambridge University Press.

Forsberg, R., Sørensen, L., & Simonsen, S. (2017). Greenland and Antarctica ice sheet mass changes and effects on global sea level. *Surveys in Geophysics*, *38*(1), 89–104. https://doi.org/10.1007/s10712-016-9398-7

García-Ibáñez, M. I., Pardo, P. C., Carracedo, L. I., Mercier, H., Lherminier, P., Ríos, A. F., & Pérez, F. F. (2015). Structure, transports and transformations of the water masses in the Atlantic Subpolar Gyre. *Progress in Oceanography*, *135*, 18–36. https://doi.org/10.1016/j.pocean.2015.03.009

Gelderloos, R., Katsman, C. A., & Drijfhout, S. S. (2011). Assessing the roles of three eddy types in restratifying the Labrador Sea after deep convection. *Journal of Physical Oceanography*, *41*(11), 2102–2119. https://doi.org/10.1175/JPO-D-11-054.1

Gelderloos, R., Straneo, F., & Katsman, C. A. (2012). Mechanisms behind the temporary shutdown of deep convection in the Labrador Sea: Lessons from the great salinity anomaly years 1968–71. *Journal of Climate*, *25*(19), 6743–6755. https://doi.org/10.1175/JCLI-D-11-00549.1

Gerdes, R., Hurka, J., Karcher, M., Kauker, F., & Köberle, C. (2005). Simulated history of convection in the Greenland and Labrador Seas, 1948–2001, *The Nordic Seas: An integrated perspective* (pp. 221–238). Washington, DC: American Geophysical Union. https://doi.org/10.1029/158GM15

Gillard, L. C., Hu, X., Myers, P. G., & Bamber, J. L. (2016). Meltwater pathways from marine terminating glaciers of the Greenland ice sheet. *Geophysical Research Letters*, *43*, 10,873–10,882. https://doi.org/10.1002/2016GL070969

Haine, T., Böning, C., Brandt, P., Fischer, J., Funk, A., Kieke, D., et al. (2008). North Atlantic Deep Water formation in the Labrador Sea, recirculation through the subpolar gyre, and discharge to the subtropics, *Arctic-Subarctic ocean fluxes* (pp. 653–701). Netherlands, Dordrecht: Springer. https://doi.org/10.1007/978-1-4020-6774-7_28

Hátún, H., Eriksen, C. C., & Rhines, P. B. (2007). Buoyant eddies entering the Labrador Sea observed with gliders and altimetry. *Journal of Physical Oceanography*, *37*(12), 2838–2854. https://doi.org/10.1175/2007JPO3567.1

Holdsworth, A. M., & Myers, P. G. (2015). The Influence of high-frequency atmospheric forcing on the circulation and deep convection of the Labrador Sea. *Journal of Climate*, *28*(12), 4980–4996. https://doi.org/10.1175/JCLI-D-14-00564.1

Holte, J., & Straneo, F. (2017). Seasonal overturning of the Labrador Sea as observed by Argo floats. *Journal of Physical Oceanography*, *47*(10), 2531–2543. https://doi.org/10.1175/JPO-D-17-0051.1

Holte, J., Talley, L. D., Gilson, J., & Roemmich, D. (2017). An Argo mixed layer climatology and database. *Geophysical Research Letters*, *44*, 5618–5626. https://doi.org/10.1002/2017GL073426

Houssais, M.-N., & Herbaut, C. (2011). Atmospheric forcing on the Canadian Arctic Archipelago freshwater outflow and implications for the Labrador Sea variability. *Journal of Geophysical Research*, *116*, C00D02. https://doi.org/10.1029/2010JC006323

Huang, R. X. (2010). Part II: Wind-driven and thermohaline circulation, *Ocean circulation: Wind-driven and thermohaline processes* (pp. 261–791). Cambridge: Cambridge University Press.

Huntington, T. G. (2006). Evidence for intensification of the global water cycle: Review and synthesis. *Journal of Hydrology*, *319*(1), 83–95. https://doi.org/10.1016/j.jhydrol.2005.07.003

Hurrell, J. W., & van Loon, H. (1997). Decadal variations in climate associated with the North Atlantic Oscillation. *Climatic Change*, *36*(3), 301–326. https://doi.org/10.1023/A:1005314315270

Jones, H., & Marshall, J. (1993). Convection with rotation in a neutral ocean: A study of open-ocean deep convection. *Journal of Physical Oceanography*, *23*(6), 1009–1039. https://doi.org/10.1175/1520-0485(1993)023<1009:CWRIAN>2.0.CO;2

Jones, H., & Marshall, J. (1997). Restratification after deep convection. *Journal of Physical Oceanography*, *27*(10), 2276–2286. https://doi.org/10.1175/1520-0485(1997)027<2276:RADC>2.0.CO;2

Josey, S. A., & Marsh, R. (2005). Surface freshwater flux variability and recent freshening of the North Atlantic in the eastern subpolar gyre. *Journal of Geophysical Research*, *110*, 2276–2287. https://doi.org/10.1029/2004JC002521

Jung, T., Serrar, S., & Wang, Q. (2014). The oceanic response to mesoscale atmospheric forcing. *Geophysical Research Letters*, *41*, 1255–1260. https://doi.org/10.1002/2013GL059040

Kawasaki, T., & Hasumi, H. (2014). Effect of freshwater from the West Greenland Current on the winter deep convection in the Labrador Sea. *Ocean Modelling*, *75*, 51–64. https://doi.org/10.1016/j.ocemod.2014.01.003

Khatiwala, S., Schlosser, P., & Visbeck, M. (2002). Rates and mechanisms of water mass transformation in the labrador sea as inferred from tracer observations. *Journal of Physical Oceanography*, *32*(2), 666–686. https://doi.org/10.1175/1520-0485(2002)032<0666:RAMOWM>2.0.CO;2

Khatiwala, S., & Visbeck, M. (2000). An estimate of the eddy-induced circulation in the Labrador Sea. *Geophysical Research Letters*, *27*(15), 2277–2280. https://doi.org/10.1029/1999GL011073

Kieke, D., Rhein, M., Stramma, L., Smethie, W. M., Bullister, J. L., & LeBel, D. A. (2006). Changes in the pool of Labrador Sea Water in the subpolar North Atlantic. *Geophysical Research Letters*, *34*, L06605. https://doi.org/10.1029/2006GL028959

Kieke, D., Rhein, M., Stramma, L., Smethie, W. M., LeBel, D. A., & Zenk, W. (2006). Changes in the CFC inventories and formation rates of Upper Labrador Sea Water, 1997–2001. *Journal of Physical Oceanography*, *36*(1), 64–86. https://doi.org/10.1175/JPO2814.1

Kieke, D., & Yashayaev, I. (2015). Studies of Labrador Sea Water formation and variability in the subpolar North Atlantic in the light of international partnership and collaboration. *Progress in Oceanography*, *132*, 220–232. https://doi.org/10.1016/j.pocean.2014.12.010

Kolstad, E. W., & Bracegirdle, T. J. (2008). Marine cold-air outbreaks in the future: An assessment of IPCC AR4 model results for the Northern Hemisphere. *Climate Dynamics*, *30*(7), 871–885. https://doi.org/10.1007/s00382-007-0331-0

Large, W. G., & Yeager, S. G. (2009). The global climatology of an interannually varying air-sea flux data set. *Climate Dynamics*, *33*(2), 341–364. https://doi.org/10.1007/s00382-008-0441-3

Laurent, D., Eric, B., & Bernard, B. (2005). A general adaptive multi-resolution approach to ocean modelling: Experiments a primitive equation model of the North Atlantic, *Adaptive mesh refinement—Theory and applications* (pp. 303–313). Berlin, Heidelberg: Springer.

Lazier, J., Hendry, R., Clarke, A., Yashayaev, I., & Rhines, P. (2002). Convection and restratification in the Labrador Sea, 1990–2000. *Deep Sea Research Part I: Oceanographic Research Papers*, *49*(10), 1819–1835. https://doi.org/10.1016/S0967-0637(02)00064-X

LeBel, D. A., Smethie, W. M., Rhein, M., Kieke, D., Fine, R. A., Bullister, J. L., et al. (2008). The formation rate of North Atlantic Deep Water and Eighteen Degree Water calculated from CFC-11 inventories observed during WOCE. *Deep Sea Research Part I: Oceanographic Research Papers*, *55*(8), 891–910. https://doi.org/10.1016/j.dsr.2008.03.009

Lilly, J. M., Rhines, P. B., Schott, F., Lavender, K., Lazier, J., Send, U., & D'Asaro, E. (2003). Observations of the Labrador Sea eddy field. *Progress in Oceanography*, *59*(1), 75–176. https://doi.org/10.1016/j.pocean.2003.08.013

Liu, C., & Wang, Z. (2014). On the response of the global subduction rate to global warming in coupled climate models. *Advances in Atmospheric Sciences*, *31*(1), 211–218. https://doi.org/10.1007/s00376-013-2323-9

Madec, G. (2008). NEMO Ocean Engine. Note du Pole de modélisation, Institut Pierre-Simon Laplace (IPSL), France.

Marsh, R. (2000). Recent variability of the North Atlantic thermohaline circulation inferred from surface heat and freshwater fluxes. *Journal of Climate*, *13*(18), 3239–3260. https://doi.org/10.1175/1520-0442(2000)013<3239:RVOTNA>2.0.CO;2

Marsh, R., Josey, S., De Nurser, A., Cuevas, B., & Coward, A. (2005). Water mass transformation in the North Atlantic over 1985–2002 simulated in an eddy-permitting model. *Ocean Science*, *1*(2), 127–144. https://doi.org/10.5194/os-1-127-2005

Marshall, J., & Schott, F. (1999). Open-ocean convection: Observations, theory, and models. *Reviews of Geophysics*, *37*(1), 1–64. https://doi.org/10.1029/98RG02739

Marzocchi, A., Hirschi, J. J.-M., Holliday, N. P., Cunningham, S. A., Blaker, A. T., & Coward, A. C. (2015). The North Atlantic subpolar circulation in an eddy-resolving global ocean model. *Journal of Marine Systems*, *142*, 126–143. https://doi.org/10.1016/j.jmarsys.2014.10.007

Masina, S., Storto, A., Ferry, N., Valdivieso, M., Haines, K., Balmaseda, M., et al. (2017). An ensemble of eddy-permitting global ocean reanalyses from the MyOcean project. *Climate Dynamics*, *49*(3), 813–841. https://doi.org/10.1007/s00382-015-2728-5

Mauritzen, C., & Häkkinen, S. (1999). On the relationship between dense water formation and the "Meridional Overturning Cell" in the North Atlantic Ocean. *Deep Sea Research Part I: Oceanographic Research Papers*, *46*(5), 877–894. https://doi.org/10.1016/S0967-0637(98)00094-6

McCartney, M. S., & Talley, L. D. (1982). The subpolar mode water of the North Atlantic Ocean. *Journal of Physical Oceanography*, *12*(11), 1169–1188. https://doi.org/10.1175/1520-0485(1982)012<1169:TSMWOT>2.0.CO;2

Müller, V., Kieke, D., Myers, P. G., Pennelly, C., & Mertens, C. (2017). Temperature flux carried by individual eddies across 47°N in the Atlantic Ocean. *Journal of Geophysical Research: Oceans*, *122*, 2441–2464. https://doi.org/10.1002/2016JC012175

Myers, P. G. (2005). Impact of freshwater from the Canadian Arctic Archipelago on Labrador Sea water formation. *Geophysical Research Letters*, *32*, L06605. https://doi.org/10.1029/2004GL022082

Myers, P. G., & Donnelly, C. (2008). Water mass transformation and formation in the Labrador Sea. *Journal of Climate*, *21*(7), 1622–1638. https://doi.org/10.1175/2007JCLI1722.1

Myers, P. G., Kulan, N., & Ribergaard, M. H. (2007). Irminger Water variability in the West Greenland Current. *Geophysical Research Letters*, *34*, L17601. https://doi.org/10.1029/2007GL030419

Nash, S., & Hartnett, M. (2014). Development of a nested coastal circulation model: Boundary error reduction. *Environmental Modelling & Software*, *53*(Supplement C), 65–80. https://doi.org/10.1016/j.envsoft.2013.11.007

Pickart, R. S., & Spall, M. A. (2007). Impact of Labrador Sea convection on the North Atlantic Meridional Overturning Circulation. *Journal of Physical Oceanography*, *37*(9), 2207–2227. https://doi.org/10.1175/JPO3178.1

Qiu, B., & Huang, R. X. (1995). Ventilation of the North Atlantic and North Pacific: Subduction versus obduction. *Journal of Physical Oceanography*, *25*(10), 2374–2390. https://doi.org/10.1175/1520-0485(1995)025<2374:VOTNAA>2.0.CO;2

Rao, S. T., Zalewsky, E., & Zurbenko, I. G. (1994). Detecting and tracking changes in ozone air quality. *Journal of the Air & Waste Management Association*, *44*(9), 1089–1092. https://doi.org/10.1080/10473289.1994.10467303

Rattan, S., Myers, P. G., Tréguier, A.-M., Theetten, S., Biastoch, A., & Böning, C. (2010). Towards an understanding of Labrador Sea salinity drift in eddy-permitting simulations. *Ocean Modelling*, *35*(1), 77–88. https://doi.org/10.1016/j.ocemod.2010.06.007

Rhein, M., Fischer, J., Smethie, W. M., Smythe-Wright, D., Weiss, R. F., Mertens, C., et al. (2002). Labrador sea water: Pathways, CFC inventory, and formation rates. *Journal of Physical Oceanography*, *32*(2), 648–665. https://doi.org/10.1175/1520-0485(2002)032<0648:LSWPCI>2.0.CO;2

Rhein, M., Kieke, D., Hüttl-Kabus, S., Roessler, A., Mertens, C., Meissner, R., et al. (2011). Deep water formation, the subpolar gyre, and the Meridional Overturning Circulation in the subpolar North Atlantic. *Deep Sea Research Part II: Topical Studies in Oceanography*, *58*(17–18), 1819–1832. https://doi.org/10.1016/j.dsr2.2010.10.061

Rhein, M., Kieke, D., & Steinfeldt, R. (2015). Advection of North Atlantic Deep Water from the Labrador Sea to the Southern Hemisphere. *Journal of Geophysical Research: Oceans*, *120*, 2471–2487. https://doi.org/10.1002/2014JC010605

Sabine, C. L., Feely, R. A., Gruber, N., Key, R. M., Lee, K., Bullister, J. L., et al. (2004). The oceanic sink for anthropogenic $CO_2$. *Science*, *305*(5682), 367–371. https://doi.org/10.1126/science.1097403

Schulze, L. M., Pickart, R. S., & Moore, G. W. K. (2016). Atmospheric forcing during active convection in the Labrador Sea and its impact on mixed-layer depth. *Journal of Geophysical Research: Oceans*, *121*, 6978–6992. https://doi.org/10.1002/2015JC011607

Smeed, D., McCarthy, G., Rayner, D., Moat, B. I., Johns, W. E., Baringer, M. O., & Meinen, C. S. (2017). *Atlantic Meridional Overturning Circulation Observed by the RAPID-MOCHA-WBTS Array at 26°N from 2004 to 2017*, (RAPID-Meridional Overturning Circulation and Heatflux Array-Western Boundary Time Series). UK: British Oceanographic Data Centre - Natural Environment Research Council. https://doi.org/10.5285/5acfd143-1104-7b58-e053-6c86abc0d94b

Smith, G. C., Roy, F., Mann, P., Dupont, F., Brasnett, B., Lemieux, J.-F., et al. (2014). A new atmospheric dataset for forcing ice–ocean models: Evaluation of reforecasts using the Canadian global deterministic prediction system. *Quarterly Journal of the Royal Meteorological Society*, *140*(680), 881–894. https://doi.org/10.1002/qj.2194

Speer, K., & Tziperman, E. (1992). Rates of water mass formation in the North Atlantic Ocean. *Journal of Physical Oceanography*, *22*(1), 93–104. https://doi.org/10.1175/1520-0485(1992)022<0093:ROWMFI>2.0.CO;2

Steinfeldt, R., Rhein, M., Bullister, J. L., & Tanhua, T. (2009). Inventory changes in anthropogenic carbon from 1997–2003 in the Atlantic Ocean between 20°S and 65°N. *Global Biogeochemical Cycles*, *23*, GB3010. https://doi.org/10.1029/2008GB003311

Stendardo, I., & Gruber, N. (2012). Oxygen trends over five decades in the North Atlantic. *Journal of Geophysical Research*, *117*, C11004. https://doi.org/10.1029/2012JC007909

Stramma, L., Kieke, D., Rhein, M., Schott, F., Yashayaev, I., & Koltermann, K. P. (2004). Deep water changes at the western boundary of the subpolar North Atlantic during 1996 to 2001. *Deep Sea Research Part I: Oceanographic Research Papers*, *51*(8), 1033–1056. https://doi.org/10.1016/j.dsr.2004.04.001

The Lab Sea Group (1998). The Labrador Sea Deep Convection Experiment. *Bulletin of the American Meteorological Society*, *79*(10), 2033–2058. https://doi.org/10.1175/1520-0477(1998)079<2033:TLSDCE>2.0.CO;2

Trossman, D. S., Thompson, L. A., Kelly, K. A., & Kwon, Y.-O. (2009). Estimates of North Atlantic ventilation and mode water formation for winters 2002–06. *Journal of Physical Oceanography*, *39*(10), 2600–2617. https://doi.org/10.1175/2009JPO3930.1

Våge, K., Pickart, R. S., Thierry, V., Reverdin, G., Lee, C. M., Petrie, B., et al. (2008). Surprising return of deep convection to the subpolar North Atlantic ocean in winter 2007–2008. *Nature Geoscience*, *2*, 67–72. https://doi.org/10.1038/NGEO382

van Angelen, J. H., Lenaerts, J. T. M., van den Broeke, M. R., Fettweis, X., & van Meijgaard, E. (2013). Rapid loss of firn pore space accelerates 21st century Greenland mass loss. *Geophysical Research Letters*, *40*, 2109–2113. https://doi.org/10.1002/grl.50490

Velicogna, I., Sutterley, T. C., & van den Broeke, M. R. (2014). Regional acceleration in ice mass loss from Greenland and Antarctica using GRACE time-variable gravity data. *Geophysical Research Letters*, *41*, 8130–8137. https://doi.org/10.1002/2014GL061052

Wang, G., Wang, D., Trenberth, K. E., Erfanian, A., Yu, M., Bosilovich, M. G., & Parr, D. T. (2017). The peak structure and future changes of the relationships between extreme precipitation and temperature. *Nature Climate Change*, *7*, 268–274. https://doi.org/10.1038/nclimate3239

Weijer, W., Maltrud, M. E., Hecht, M. W., Dijkstra, H. A., & Kliphuis, M. A. (2012). Response of the Atlantic Ocean circulation to Greenland ice sheet melting in a strongly-eddying ocean model. *Geophysical Research Letters*, *39*, L09606. https://doi.org/10.1029/2012GL051611

Yang, Q., Timothy, H. D., Paul, G. M., Bonin, J., Chambers, D., van den Broeke, M. R., et al. (2016). Recent increases in Arctic freshwater flux affects Labrador Sea convection and Atlantic overturning circulation. *Nature Communications*, *7*, 10525. https://doi.org/10.1038/ncomms10525

Yashayaev, I. (2007). Hydrographic changes in the Labrador Sea, 1960–2005. *Progress in Oceanography*, *73*(3), 242–276. https://doi.org/10.1016/j.pocean.2007.04.015

Yashayaev, I., Bersch, M., & van Aken, H. M. (2007). Spreading of the Labrador Sea water to the Irminger and Iceland basins. *Geophysical Research Letters*, *34*, L10602. https://doi.org/10.1029/2006GL028999

Yashayaev, I., Bersch, M., van Aken, H., & Clarke, A. (2004). A new study of the production, spreading and fate of the Labrador Sea Water in the subpolar North Atlantic. *ASOF Newsletter*, *2*, 20–23.

Yashayaev, I., & Clarke, A. (2006). Recent warming of the Labrador Sea. *AZMP Bulletin PMZA*, *5*, 12–20.

Yashayaev, I., & Dickson, B. (2008). *Transformation and fate of overflows in the northern North Atlantic, in Arctic–Subarctic ocean fluxes* (pp. 505–526). Netherlands, Dordrecht: Springer. https://doi.org/10.1007/978-1-4020-6774-7_22

Yashayaev, I., Holliday, N. P., Bersch, M., & van Aken, H. M. (2008). The history of the Labrador Sea water: Production, spreading, transformation and loss, *Arctic-subarctic ocean fluxes: Defining the role of the Northern Seas in climate* (pp. 569–612). Dordrecht: Springer. https://doi.org/10.1007/978-1-4020-6774-7_25

Yashayaev, I., & Loder, J. W. (2009). Enhanced production of Labrador Sea water in 2008. *Geophysical Research Letters*, *36*, L01606. https://doi.org/10.1029/2008GL036162

Yashayaev, I., & Loder, J. W. (2016). Recurrent replenishment of Labrador Sea Water and associated decadal-scale variability. *Journal of Geophysical Research: Oceans*, *121*, 8095–8114. https://doi.org/10.1002/2016JC012046

Yashayaev, I., & Loder, J. W. (2017). Further intensification of deep convection in the Labrador Sea in 2016. *Geophysical Research Letters*, *44*, 1429–1438. https://doi.org/10.1002/2016GL071668

Zahn, M., & von Storch, H. (2010). Decreased frequency of North Atlantic polar lows associated with future climate warming. *Nature*, *467*(7313), 309–312. https://doi.org/10.1038/nature09388

Zurbenko, I., Porter, P., Gui, R., Rao, S., Ku, J., & Eskridge, R. (1996). Detecting discontinuities in time series of upper-air data: Development and demonstration of an adaptive filter technique. *Journal of Climate*, *9*(12), 3548–3560. https://doi.org/10.1175/1520-0442(1996)009<3548:DDITSO>2.0.CO;2